bioRxiv preprint doi: https://doi.org/10.1101/2021.01.11.425814; this version posted January 11, 2021. The copyright holder for this preprint (which was not certified by peer review) is the author/funder, who has granted bioRxiv a license to display the preprint in perpetuity. It is made available under aCC-BY-NC-ND 4.0 International license.

Biophysical investigation of the dual binding surfaces of human transcription factors FOXO4 and p53

Jinwoo Kim[+], Dabin Ahn[+], and Chin-Ju Park[*]

Department of Chemistry, Gwangju Institute of Science and Technology, Gwangju, 61005, Korea

*Correspondence to: cjpark@gist.ac.kr.

[+] These authors contributed equally to this work.

bioRxiv preprint doi: https://doi.org/10.1101/2021.01.11.425814; this version posted January 11, 2021. The copyright holder for this preprint (which was not certified by peer review) is the author/funder, who has granted bioRxiv a license to display the preprint in perpetuity. It is made available under aCC-BY-NC-ND 4.0 International license.

Abstract

Cellular senescence is protective against external oncogenic stress, but its accumulation causes aging-related diseases. Forkhead box O4 (FOXO4) and p53 are human transcription factors known to promote senescence by interacting in the promyelocytic leukemia bodies. Inhibiting their binding is a strategy for inducing apoptosis of senescent cells, but the binding surfaces that mediate the interaction of FOXO4 and p53 remain elusive. Here, we investigated two binding sites involved in the interaction between FOXO4 and p53 by using NMR spectroscopy. NMR chemical shift perturbation analysis showed that the binding between FOXO4's forkhead domain (FHD) and p53's transactivation domain (TAD), and between FOXO4's C-terminal transactivation domain (CR3) and p53's DNA binding domain (DBD), mediate the FOXO4-p53 interaction. Also, we showed that the CR3-binding surface of FOXO4 FHD interacts with p53 TAD2, and four residues of FOXO4 CR3 interact with the DNA-binding surface of p53 DBD. Further isothermal titration calorimetry experiments showed that the FOXO4 FHD-p53 TAD interaction takes precedence with high affinity and that the FOXO4 CR3-p53 DBD interaction follows. This work provides structural information at the molecular level that is key to understanding the interplay of two proteins responsible for cellular senescence.

Keywords

cellular senescence; transcription factor; protein-protein interaction; NMR; isothermal titration calorimetry

Abbreviations

FOXO4, forkhead box O4; FHD, forkhead domain; TAD, transactivation domain; DBD, DNA binding domain; NMR, nuclear magnetic resonance; HSQC, heteronuclear single quantum coherence; CSP, chemical shift perturbation; ITC, isothermal titration calorimetry; PPI, protein-protein interaction; TF, transcription factor

bioRxiv preprint doi: https://doi.org/10.1101/2021.01.11.425814; this version posted January 11, 2021. The copyright holder for this preprint (which was not certified by peer review) is the author/funder, who has granted bioRxiv a license to display the preprint in perpetuity. It is made available under aCC-BY-NC-ND 4.0 International license.

Introduction

The forkhead box class O (FOXO) subfamily consists of four transcription factors (TFs), FOXO1, FOXO3a, FOXO4, and FOXO6, which share a conserved DNA binding domain called the forkhead domain (FHD).[1,2] As TFs, FOXO proteins participate in various cellular processes such as regulation of the cell cycle, cell survival, metabolism, and tumorigenesis by controlling the expression of their target genes.[3-10] In particular, FOXOs are known to be important regulators of cellular senescence.[11] Cellular senescence proceeds in response to the induction of permanent cell cycle arrest regardless of the presence of growth factors. Therefore, senescent cells avoid apoptosis and induce a pro-inflammatory environment that affects the neighboring cells.[12-14] Unlike apoptotic cells, which are immediately removed, senescent cells are maintained for a long time, and their accumulation accelerates aging and causes senescence-associated diseases such as type □ diabetes[15], osteoarthritis[16], atherosclerosis[17], neurodegenerative disorders[18], and cancers[13,14,19].

FOXO4 is a member of the FOXO subfamily and a factor involved in cellular senescence.[11] Like other FOXOs, it has five domains: the FHD, a nuclear localization sequence (NLS), a nuclear export sequence (NES), and two transactivation domains called CR1 and CR3 (Figure 1A).[20] The CR3 domain is also known as the transactivation domain (TAD). Only the FHD, which binds to two conserved DNA sequences, 5'-TTGTTTAC-3', named the Daf-16 family member-binding element (DBE)[21,22], and 5'-(C/A)(A/C)AAA(C/T)AA -3', named the insulin-responsive sequence (IRE)[22], has defined structure. Other than the FHD, most regions of FOXO4 exist in a intrinsically disordered state, including CR3.[23] After acute DNA damage, the expression level of FOXO4 gradually increases, which induces cellular senescence compared to apoptosis and suppresses the apoptosis response, allowing the viability of senescent cells to be maintained.[11] Inhibition of FOXO4 expression causes the release of mitochondrial cytochrome C and BAX/BAK-dependent caspase-3 cleavage, leading to reduced cell viability and density. Also, an increase in reactive oxygen species by oxidative stress triggers phosphorylation of c-Jun N-terminal kinase (JNK) through the mitogen□activated protein kinase kinase (MEK) pathway.[7] In turn, phosphorylated JNK phosphorylates and activates FOXO4.[6-8] Activated FOXO4 increases the transcription of p21, which is involved in cell cycle arrest and promotes cellular senescence.[7,24]

As senescence progresses, FOXO4 is gradually accumulated into euchromatin foci and interacts with activated p53 in promyelocytic leukemia bodies at the DNA damage site.[11] p53 is a homo-tetrameric transcription factor that regulates various target genes and participates in the control of several cellular processes, including cell cycle arrest, apoptosis, and senescence.[25-29] The N-terminal transactivation domain (TAD), a proline-rich domain (PRD), a DNA-binding domain (DBD), a tetramerization domain (TA), and the C-terminal negative regulatory domain (NRD) are components of p53 (Figure

bioRxiv preprint doi: https://doi.org/10.1101/2021.01.11.425814; this version posted January 11, 2021. The copyright holder for this preprint (which was not certified by peer review) is the author/funder, who has granted bioRxiv a license to display the preprint in perpetuity. It is made available under aCC-BY-NC-ND 4.0 International license.

1B). With these multiple domains, p53 can cooperate with numerous partners and behaves as a central protein-protein interaction (PPI) hub in biological systems.[30] Although p53 and FOXOs specifically recognize different sequences in promoter sites, they have common downstream target genes such as WIF1, FASLG, GADD45, and PA21.[31,32] In particular, when FOXO4 and p53 bind each other within the nucleus of senescent cells, the nuclear exclusion of p53 is disrupted, and the transcription of the p21 gene is activated.[11,33] Overexpressed p21 participates in the cellular senescence process by arresting the cell cycle through negative regulation of the G1/S and G2/M transitions.[34,35] In addition, since the exclusion of p53 is restrained, the apoptosis process induced by p53 cannot proceed appropriately in mitochondria, accelerating cellular senescence.[36] Therefore, it has been proposed to modulate the FOXO4-p53 interaction as a target for treating aging. Baar *et al.* developed the FOXO4-D-retro-inverso (FOXO4-DRI) peptide as a way of introducing D-amino acids in a retro-reversed sequence of the FOXO4 FHD N-terminus.[11] They attempted to inhibit the binding between FOXO4 and p53 through FOXO4-DRI, and demonstrated that the introduction of this peptide induces death of senescent cells.

Despite the increasing interest in the interaction between FOXO4 and p53, which are involved in cellular senescence and apoptosis, structural information is insufficient. Since it is known that the FOXO4 FHD domain binds a wide region of the p53 sequence, including the TAD, PRD, and DBD,[11] it is necessary to clarify the binding site further to understand the FOXO4-p53 complex. Therefore, we investigated the interaction of FOXO4 and p53 at the molecular level. The FHD and CR3 domains of FOXO3a, which have high sequence similarity to FOXO4, bind to the DBD of p53.[37] Also, CR3 of the FOXO proteins plays a role in recruitment of co-activators such as CBP/p300.[37,38] Therefore, we selected FHD and CR3 of FOXO4 as potential candidates for p53 binding. The DBD and TAD regions of p53 interact with many proteins and control various signaling pathways[37,39-46], and thus these two domains were used as candidates for binding to FOXO4. In this work, we demonstrated that FOXO4's FHD and CR3 directly bind to TAD and DBD of p53, respectively, using nuclear magnetic resonance (NMR) spectroscopy. Alanine mutation analysis of FOXO4 CR3 showed that the binding to p53 DBD occurs on wide and shallow surfaces. In addition, a binding affinity comparison using isothermal titration calorimetry (ITC) experiments showed that FOXO4 CR3-p53 DBD binding takes precedence over FOXO4 FHD-p53 TAD during the formation of the FOXO4-p53 complex. This biophysical characterization of the FOXO4-p53 interaction is expected to contribute to new strategies for the development of inhibitors of cellular senescence.

bioRxiv preprint doi: https://doi.org/10.1101/2021.01.11.425814; this version posted January 11, 2021. The copyright holder for this preprint (which was not certified by peer review) is the author/funder, who has granted bioRxiv a license to display the preprint in perpetuity. It is made available under aCC-BY-NC-ND 4.0 International license.

Results

FOXO4 FHD prefers binding to p53 TAD

Previously, the binding of FOXO4 FHD to p53 was studied using NMR spectroscopy, but the information on the domain of p53 and the region of FOXO4 FHD required for this binding was ambiguous.[11] Thus, it is necessary to accurately identify the domain used for the interaction of p53 with FOXO4 FHD. So, we prepared ^{15}N-labeled FOXO4 FHD and performed chemical shift perturbation (CSP) analysis with p53 TAD or DBD to observe the binding between intermolecular domains. CSP showed which residues of p53 were involved in the interaction with FOXO4 FHD when equimolar amounts of the respective domains were present. The ^{1}H-^{15}N amide cross peaks of ^{15}N-labeled FOXO4 FHD were assigned based on the previously published backbone assignment.[47] In the NMR titration between ^{15}N-labeled FOXO4 FHD and p53 TAD, several residues were found to undergo a large change (Figure 2A and 2C). Residues G102, S105, and Y137 of FOXO4 FHD were perturbed by more than the average + 2 standard deviations (σ), and residues W101ε, Q104, Y106, L160, K163, T172, and E183 were also changed relatively significantly (average + 1σ). They were all in a pocket-like space formed in the crevice between the N-terminal loop and α-helices H1, H4, and H3, except for T172, which is located in the flexible wing W1 (Figure 2E). In particular, W101ε, Q104, S105, L160, and T172 are FOXO4 FHD residues that also participate in the intramolecular interaction of FOXO4 FHD with CR3.[48] It can be assumed that FOXO4 CR3 can compete with the formation of the FOXO4-p53 complex. In addition, a large perturbation of several hydrophobic residues was observed, including three aromatic residues (Y137, W101ε, Y106), which may mean that hydrophobic interactions are involved in the binding of FOXO4 FHD and p53 TAD. Next, we performed NMR titration between ^{15}N-labeled FOXO4 FHD and p53 DBD (Figure 2B and 2D). In contrast to experiments with p53 TAD, no residues of FOXO4 FHD were found that were significantly perturbed by p53 DBD. Also, the average value of CSP of FOXO4 FHD caused by p53 DBD was about 0.004, which was much smaller than that caused by p53 TAD, 0.154. These results suggest that p53 interacts with FOXO4 FHD via its TAD rather than DBD. It is expected that p53 TAD binds in the pocket provided by FOXO4 FHD, interfering with the formation of the intramolecular complex of FOXO4 and inducing the FOXO4-p53 interaction.

p53 helix TAD2 is responsible for the interaction with FOXO4 FHD

As shown in Figure 1B, p53 TAD contains two α-helices, which are named TAD1 and TAD2, respectively. They are adjacent in position but are functionally independent. For example, TAD1 is more important than TAD2 in p53-dependent transactivation and is essential for DNA damage-induced G1 arrest but not for RAS-induced senescence in fibroblasts,[49] while TAD2 predominates over TAD1 in binding to mediator complex subunit 25 (MED25).[50] On the other hand, sometimes

bioRxiv preprint doi: https://doi.org/10.1101/2021.01.11.425814; this version posted January 11, 2021. The copyright holder for this preprint (which was not certified by peer review) is the author/funder, who has granted bioRxiv a license to display the preprint in perpetuity. It is made available under aCC-BY-NC-ND 4.0 International license.

their role is cooperative from a PPI perspective. In p53 intramolecular interaction, both TAD1 and TAD2 participate in binding to p53 DBD.[51] Thus, information on the behavior of TAD1 and TAD2 is necessary to understand the interaction of FOXO4 FHD with p53 TAD precisely. We titrated FOXO4 FHD into ^{15}N-labeled p53 TAD and performed NMR CSP analysis to observe whether TAD1 and TAD2 are cooperative or independent in FOXO4 binding. In Figure 3A and 3C, the CSP of TAD1 and its nearby residues was relatively small. There were no residues that underwent a change of more than the average + 1σ. On the other hand, TAD2 had a completely different trend. Residues D48, E51, Q52, W53, and F54 in TAD2 had perturbation of more than the average + 2σ, and it was the same for neighboring T55. I50 also underwent a relatively large change. These results strongly indicate that p53 TAD2 is dominantly involved in the binding between FOXO4 FHD and p53 TAD, whereas TAD1 does not participate or has a minor role. Additionally, changes of A39, M40, D42, L43, L45, and S46 near TAD2's N-terminus were observed, which may imply that not only TAD2 but also its surroundings participate in the interaction with FOXO4 FHD, or their structural environment is changed by the interaction. As found in FOXO4 FHD, p53 TAD2 and its surroundings showed changes in aromatic residues (W53 and F54), and perturbation of several aliphatic residues (L32, A39, M40, M44, L45, I50) was observed. This underscores the hydrophobic portion of the interaction. It is also noteworthy that several acidic residues were perturbed in p53 TAD2 (D48, E51, and D57), which are complementary to the basic amino acids K139, K141, K151, R155, H156, and H161 located on the FOXO4 FHD H1, H3, and H4 binding surface (Figure 2E). Also, FOXO4 FHD is positively charged (pI = 10.11) and p53 TAD (pI = 3.39) is negatively charged. Thus, it can be reasonably expected that specific electrostatic contacts contribute to the interaction between FOXO4 FHD and p53 TAD2. We additionally performed an NMR titration between ^{15}N-labeled p53 DBD and FOXO4 FHD, but did not find any significantly perturbed residues of p53 DBD, similar to the previous experiment with ^{15}N-labeled with FOXO4 FHD (Figure 3B and 3D). Taken together, the results of NMR titrations with reciprocal ^{15}N isotope labeling show that p53 TAD rather than DBD generates the interaction between FOXO4 FHD and p53, and in particular p53 TAD2 is involved in the complex.

FOXO4 CR3 also participates in the interaction with p53

FOXO4 CR3 domain is an intrinsically disordered region, which is considered challenging to study structurally, but in recent research using NMR spectroscopy, we successfully observed that aliphatic amino acids of this domain participate in an intramolecular interaction with FHD at the molecular level.[48] This means that the FOXO4 CR3 domain, despite being intrinsically disordered, can be involved in interplay with other elements, including the intramolecular unit. Previous studies have shown that the CR3 domain of FOXO3a interacts with intermolecular partners, and p53 DBD is one of them.[37,38] FOXO4 and FOXO3a CR3 domains have high sequence homogeneity.[48] Thus, we tried to

bioRxiv preprint doi: https://doi.org/10.1101/2021.01.11.425814; this version posted January 11, 2021. The copyright holder for this preprint (which was not certified by peer review) is the author/funder, who has granted bioRxiv a license to display the preprint in perpetuity. It is made available under aCC-BY-NC-ND 4.0 International license.

determine whether the FOXO4 CR3 is a potential binding partner of p53 DBD. ^{15}N-labeled FOXO4 CR3 was prepared and used to perform NMR titration and CSP analysis with p53 DBD. The backbone assignment was reported previously.[48] As shown in Figure 4, the CSP of FOXO4 CR3 residues M476, I487, S488, and M491 was observed to be greater than the average + 1σ. These are mostly aliphatic amino acids, from which we can infer that FOXO4 CR3 and p53 DBD interact by hydrophobic attraction. Residues Y475, N478, L479, E480, C481, D484, I486, L490, and D492 also appeared to undergo relatively large perturbation. This list is a mixture of aliphatic and acidic amino acids, suggesting that the interaction between FOXO4 TAD and p53 DBD is affected by both hydrophobic and electrostatic attractions, similar to FOXO4 FHD-p53 TAD binding.

Binding surfaces of p53 DBD to DNA and to FOXO4 CR3 overlap

While the main role of p53 DBD is binding to its specific DNA sequence of 5'-PuPuPuC(A/T)(T/A)GPyPyPy-3' (Pu, purine; Yy, pyrimidne),[52] the domain also participates in an intramolecular PPI with p53 TAD, as well as intermolecular PPI with BcL-$_{XL}$[53] and Hsp90.[54] Therefore, p53 DBD is considered one of the vital domains for PPI of p53. We tried to characterize the FOXO4 CR3 binding region in p53 DBD by titrating FOXO4 CR3 into ^{15}N-labeled p53 DBD. The assignment of the ^{1}H-^{15}N HSQC spectrum was based on previous research.[55] As shown in Figure 5A and 5B, residues Y126 and S127 of β-strand S2 experienced a large CSP of more than the average + 2σ, and the CSP of A138 between S2' and S3 was also significant. α-Helix H3 and its surrounding residues C277, K291, K292, and G293 also underwent significant perturbations. Several residues that underwent a change of the average + 1σ or more were also observed, but these were spread throughout the structure. In the 3D solution structure of p53 (PDB ID: 2FEJ),[56] the positions of α-helix H3 and β-strand S2 are adjacent to each other (Figure 5C). Our CSP data suggest that p53 DBD interacts with FOXO4CR3 through its H3 and S2 regions and neighboring surfaces. Moreover, perturbation of the basic amino acids of α-helix H3, K291, K292, and R283, indicates that electrostatic attraction is involved in the intermolecular interaction between the two domains, and which is consistent with the insight of the NMR titration experiment between ^{15}N-labeled FOXO4 CR3 and p53 DBD (Figure 4). It is noteworthy that the α-helix H3 of p53 DBD participates in the binding of FOXO4 CR3 because this α-helix also participates in the specific DNA binding of p53. According to the crystal structure of the complex between p53 and DNA (PDB ID: 3Q05) (Figure 5D)[57], residues K120 and S121 located at loop L1 of the DBD, and residues C277, R280, and R283 located at α-helix H3, serve as contact points with DNA. C277 and R283 are also residues in which large CSPs were caused by the addition of FOXO4 CR3. The overlapping of these residues implies that there might be competition between FOXO4 CR3 and DNA for p53 binding.

bioRxiv preprint doi: https://doi.org/10.1101/2021.01.11.425814; this version posted January 11, 2021. The copyright holder for this preprint (which was not certified by peer review) is the author/funder, who has granted bioRxiv a license to display the preprint in perpetuity. It is made available under aCC-BY-NC-ND 4.0 International license.

The interaction between FOXO4 CR3 and p53 DBD is mediated over a wide surface

In the above experiments, the largest CSPs in FOXO4 CR3 induced by p53 DBD were limited to four residues, M476, I487, S488, and M491 (Figure 4B). This differs from the experiment with ^{15}N-labeled p53 TAD and FOXO4 FHD, where large CSPs were concentrated in one α-helix (TAD2) (Figure 3C). We hypothesized that because of the intrinsically disordered nature of FOXO4 CR3, the binding surface might not be highly refined. In order to evaluate the role of the four most perturbed residues for the binding of p53 DBD, we introduced alanine mutations for CR3 residues M476, I487, S488, and M491 and performed NMR titration experiments with ^{15}N-labeled p53 DBD (Figure 6). As shown in the CSP analysis of ^{15}N-labeled p53 DBD and the FOXO4 CR3 mutants, the perturbation of residues belonging to β-strand S2 and α-helix H3, which were observed as important regions for binding to wild-type FOXO4 CR3, was relatively well maintained in mutants I487A, S488A, and M491A (Figure 6B, 6C, and 6D). Although CSPs of S127 and A138 located in β-strand S2 and its surrounding residues decreased in magnitude, the aromatic amino acid Y126 still maintained a CSP above the average + 2σ of the experiment with wild-type CR3 protein. CSPs of C277, K291, K292, and G293, which are important α-helix H3 residues in the FOXO4 CR3 binding, also maintained high values. On the other hand, the FOXO4 CR3 M476A mutant showed a different tendency than the others. In Figure 6A, the CSP of the key residues of β-strand S2 was significantly reduced. Even the perturbation of Y126 was markedly reduced. In addition, the CSP of residue C277, a residue structurally adjacent to β-strand S2, was also relatively small compared to the other three cases. This data indicates that M476 of FOXO4 CR3 is an important residue for the binding of p53 DBD β-strand S2. However, as the perturbation of residues belonging to α-helix H3 is relatively maintained, this mutation does not seem to completely abolish the binding between FOXO4 CR3-p53 DBD. Therefore, we found that the FOXO4 CR3-p53 DBD interaction is distributed across several residues in CR3, such that the interaction is maintained if one of them is missing. Thus, it can be inferred that the flexible FOXO4 CR3, without distinct secondary structure, can provide various contact points over a wide surface during the binding with p53 DBD.

Thermodynamic analysis of FOXO4-p53 dual binding surface

We performed ITC experiments to quantify the thermodynamic profiles of the binding between domains that contribute to the formation of the FOXO4-p53 complex. As shown in Figure 7A, the binding affinity between FOXO4 FHD and p53 TAD has a binding affinity of 2.19 ± 0.06 μM. The ΔG and ΔH values for this reaction were calculated as -7.15 ± 0.46 kcal/mol and 12.29 ± 2.06 kcal/mol, respectively (Figure 7B). This means that the reaction takes place in the form of a spontaneous endothermic reaction. Also, the value of stoichiometry (n) was determined to be 1.04, suggesting that they participate in the binding at a 1:1 ratio (Figure 7A). The positive change in

bioRxiv preprint doi: https://doi.org/10.1101/2021.01.11.425814; this version posted January 11, 2021. The copyright holder for this preprint (which was not certified by peer review) is the author/funder, who has granted bioRxiv a license to display the preprint in perpetuity. It is made available under aCC-BY-NC-ND 4.0 International license.

entropy (ΔS) observed appears to be due to the hydrophobic attraction between the two domains causing the scatter of water molecules on the binding surface. This suggestion is supported by the NMR experiments, in which the perturbation several hydrophobic amino acids was observed between FOXO FHD and p53 TAD. These experimental values are similar to those of the previously described thermodynamic profile of the intramolecular interaction of FOXO4, although there are differences in absolute quantities.[48] This means that the binding of FOXO4 FHD to p53 TAD occurs with a mechanism similar to contact with the CR3 domain.

FOXO4 CR3 and p53 DBD interact with different thermodynamic characteristics. The binding affinity was measured to be 10.26 ± 0.64 μM, and ΔG and ΔH were -6.91 ± 0.35 kcal/mol and -1.11 ± 0.61 kcal/mol, which is assumed to be a spontaneous exothermic reaction. The value of n was 0.781, which is a little less than 1, but it can be expected that the two domains interact in a 1:1 ratio. The ΔS was positive, the same as in the FOXO4 FHD-p53 TAD experiment, but the magnitude of the change was smaller. Taken together, the FOXO4 FHD-p53 TAD interaction has a K_d value that is about 4.7 times lower than the FOXO4 CR3-p53 DBD interaction. This means that when FOXO4 and p53 are adjacent, the binding of FOXO4 FHD-p53 TAD takes precedence over the FOXO4 CR3-p53 DBD binding. However, if FOXO4 FHD-p53 TAD interaction is not possible due to other factors (e.g., FOXO4 FHD binds to DNA), the interaction of FOXO4 CR3-p53 DBD may be an alternative means of seeding the formation of the FOXO4-p53 complex.

bioRxiv preprint doi: https://doi.org/10.1101/2021.01.11.425814; this version posted January 11, 2021. The copyright holder for this preprint (which was not certified by peer review) is the author/funder, who has granted bioRxiv a license to display the preprint in perpetuity. It is made available under aCC-BY-NC-ND 4.0 International license.

Discussion

FOXO4 and p53 play a pivotal role in cellular senescence/apoptosis.[11,25] In senescent cells, FOXO4 is elevated and contributes to maintaining cell viability.[11] As senescence progresses, FOXO4 and p53 co-localize in the promyelocytic leukemia bodies and share roles such as inducing transcriptional activity of p21.[11,33] Thus, the interaction between FOXO4 and p53 is expected to play a direct role in cellular senescence. In fact, a peptide-based inhibitor that mimics a part of FOXO4 FHD induced p53-dependent apoptosis through binding to p53.[11] Therefore, in order to understand the mechanism of cell lifespan and to control it appropriately, information on the molecular level of FOXO4-p53 binding is required. In this study, we expanded the structural understanding of the interaction between FOXO4 and p53.

In previous studies, it was shown that the FHD of FOXO4 recognizes p53 (1-312 amino acids).[11] Here we were able to specify that the p53 TAD2 is a key region for the interaction with FOXO4 FHD (Figure 3C). Interestingly, MDM2, which induces ubiquitination and degradation of p53, interacts with the TAD1 sequence of p53.[58] This means that p53-MDM2 binding inhibits the activation of p53, as opposed to the role of FOXO4 in inducing the activation of senescence factors in cooperation with p53 in the nucleus. Since the binding site of p53 is not shared by FOXO4 and MDM2, it can be expected that these two proteins with opposing roles may bind simultaneously with p53. However, the distance between TAD1 and TAD2 is close (Figure 1B), and FOXO4 and MDM2 are relatively large proteins, about 53.7 kDa and 55.2 kDa, respectively, so steric collisions may prevent them from interacting with p53 simultaneously. In other words, FOXO4 and MDM2 proteins compete for interaction with p53. Therefore, the activity of p53 seems to be different depending on which protein partner interacts. In the FOXO4-bound state, activation is expected to contribute to cellular senescence, whereas in the MDM2-bound state, p53 is expected to undergo nuclear export and degradation. In the cell, it is thought that the expression of FOXO4 and MDM2 is regulated in a balanced manner according to external conditions, and according to this, the role of p53 is different, and the lifespan of the cell could be determined.

We found that p53 TAD binds to the pocket-like space between the N-terminal loop of FOXO4 FHD and α-helices H1, H3, and H4 through NMR titration experiments with ^{15}N-labeled FOXO4 FHD and p53 TAD (Figure 2E). In previous work, we have shown that the FOXO4 CR3 domain can bind intramolecularly to a large surface formed by the N-terminal loop, α-helices H1 and H3, β-strand S2, and wing W1 of FOXO4 FHD.[48] It is suggestive that most of the p53 TAD binding region is contained in the FOXO4 CR3 domain binding region. The sites even have large CSP values common for Q104 of the N-terminal loop, S105 of α-helix H1, and L160 of α-helix H3. Also, in the ITC experiment, the thermodynamic parameters observed for FOXO4 FHD-p53 TAD binding were similar to those

bioRxiv preprint doi: https://doi.org/10.1101/2021.01.11.425814; this version posted January 11, 2021. The copyright holder for this preprint (which was not certified by peer review) is the author/funder, who has granted bioRxiv a license to display the preprint in perpetuity. It is made available under aCC-BY-NC-ND 4.0 International license.

previously described for FOXO4 FHD-FOXO4 CR3 binding (Figure 7B).[48] This implies that FOXO4 CR3 and p53 TAD compete for FOXO4 FHD. However, by comparison of absolute values, we could easily anticipate that the intramolecular interaction of FOXO4 is predominant to the intermolecular interaction. First, the two experiments showed a significant difference in K_d values. FOXO4 FHD-FOXO4 CR3 had a high binding affinity of about 0.22 μM,[48] whereas FOXO4 FHD-p53 TAD had a K_d of 2.19 ± 0.06 μM, which is almost ten times lower. Second, the ΔG of FOXO4 intramolecular binding was measured as -9.13 kcal/mol, which is relatively lower than that of the FOXO4 FHD-p53 TAD interaction. These differences mean that the binding between the two domains of FOXO4, FHD and CR3, is more substantial and forms a thermodynamically stable complex. Therefore, FOXO4 FHD appears to favor interaction with FOXO4 CR3, compared to external p53 TAD, when exposed in a free state. Nevertheless, the intermolecular interaction of FOXO4 FHD-p53 TAD could be biologically meaningful. In particular, as mentioned above, the expression level of FOXO4 in senescent cells increases.[11] In this circumstance, since the number of FOXO4 molecules is sufficiently large in the nucleus, an opportunity for intermolecular binding with p53 may be given despite the predominance of the intramolecular interaction. In turn, p53 bound to FOXO4 cannot be released out of the nucleus, and eventually, the activation of p53 associated with cellular senescence seems to be maintained.

The binding of FOXO4 CR3 and p53 DBD has significance in that it can provide the second junction that can enhance the FOXO4-p53 interaction in addition to the primary binding between FOXO4 FHD and p53 TAD. NMR titrations through reciprocal ^{15}N labeling showed that four FOXO4 CR3 amino acids (M476, I487, S488, and M491) are required to interact with the p53 DBD α-helix H3 and its surrounding residues (Figures 4 and 5). α-Helix H3 of p53 DBD participates in DNA binding (Figure 5D),[57] and also in the interaction with p53 TAD,[51] and is in one of the pivotal regions for the various molecular interactions of p53. This suggests that FOXO4 CR3 may inhibit the binding between p53 DBD and DNA or p53 DBD and p53 TAD, but, similar to the previous case of FOXO4 FHD-p53 TAD, the binding affinity between FOXO4 CR3 and p53 DBD is low, about 10.26 μM (Figure 7B), so the effect of such interference is expected to be almost impossible. However, in FOXO4 crowded conditions, it might be possible to provide an additional contact for the FOXO4-p53 interaction with the FOXO4 FHD-p53 TAD binding. It has been recognized that weak and transient PPIs with micromolar to millimolar range binding affinity can play an important role in cell signaling and regulatory and response mechanisms by modulating the bound and unbound state populations between the two molecules.[59-61] Therefore, we suggest that binding between FOXO4 CR3 and p53 DBD, which is relatively weaker than the intramolecular interaction or the binding of the other

bioRxiv preprint doi: https://doi.org/10.1101/2021.01.11.425814; this version posted January 11, 2021. The copyright holder for this preprint (which was not certified by peer review) is the author/funder, who has granted bioRxiv a license to display the preprint in perpetuity. It is made available under aCC-BY-NC-ND 4.0 International license.

domains of FOXO4 and p53, can be a factor responsible for the maintenance of senescent cells along with the FOXO4 FHD-p53 TAD interaction.

The interaction of FOXO4 and p53 with two binding interfaces through a combination of their DNA-binding and transactivation domains is expected to bring benefits to transcription in senescent cells. Interestingly, the FOXO4 target DNA sequence and two p53 binding DNA sites are adjacent within the promoter of the p21 gene, which accelerates cellular senescence.[30] The mechanism for the cooperation of FOXO4 and p53 on the transcription of p21 is unknown, but we propose that the interaction of the two proteins contributes to the activation of p21 transcription as shown in the following three models (Figure 8). (a) When p53 is bound to the p21 promoter, p53 DBD is in contact with DNA, so p53 TAD is freely exposed in the nucleus and recruits FOXO4 to the p21 promoter through interaction with FOXO4 FHD. Afterward, FOXO4 FHD searches for its target sequence in the p21 promoter through rearrangement. (b) When FOXO4 FHD binds to the p21 promoter, FOXO4 CR3 exists in the free state and has an opportunity to attach to p53 DBD. In turn, p53 DBD is transferred to the p53 binding site of the p21 promoter. (c) When FOXO4 and p53 exist in a complex, one protein binds to the p21 promoter site through its DNA binding domain, and the remaining proteins sequentially search for DNA sequences that contact them. As a result, freely exposed p53 TAD and FOXO4 CR3 bind to transcription co-activators such as CBP/p300 and initiate transcription of p21. This dual binding at the p21 promoter seems to contribute to forming a stable transcription preinitiation complex in way that has an advantage over the single TF. In fact, studies have shown that cooperation of multiple TFs are necessary for gene activation.[62,63] Therefore, it would be meaningful to study the FOXO4-p53-DNA complex to determine how the interaction between FOXO4 and p53 contributes to this DNA binding and initiates p21 transcription in senescent cells.

As mentioned above, the development of an inhibitor that interferes with the interface of the FOXO4-p53 interaction has recently progressed. The FOXO4-DRI peptide, a mimetic of the FOXO4 FHD N-terminus, defended cells from senescence by blocking the binding of p53 and FOXO4.[11] In that study, the authors were not able to determine where the peptide targets p53 specifically. Our FOXO4 FHD-p53 TAD NMR titration results (Figure 2C and 3C) suggest that FOXO4-DRI peptide everts its inhibitory effect through binding to p53 TAD2. In other words, this inhibitor appears to regulate p53 activation in senescent cells by interrupting contact with co-activators of p53 instead of with DNA binding. It will be interesting to conduct studies that introduce and apply this inhibitor to deal with various p53-related diseases. On the other hand, we found in this study that the interaction of FOXO4 and p53 involves a dual interface. This implies that the binding of FOXO4 CR3-p53 DBD can be targeted along with FOXO4 FHD-p53 TAD to inhibit their interaction. We observed that four residues

bioRxiv preprint doi: https://doi.org/10.1101/2021.01.11.425814; this version posted January 11, 2021. The copyright holder for this preprint (which was not certified by peer review) is the author/funder, who has granted bioRxiv a license to display the preprint in perpetuity. It is made available under aCC-BY-NC-ND 4.0 International license.

of FOXO4 CR3 are important for the interaction with p53 (Figure 4), but it seems that there is no dominant involvement of a specific residue because this interaction is expected to be a binding across a wide surface (Figure 6). This implies that inhibitors targeting the FOXO4 CR3-p53 DBD binding are difficult to achieve with small molecules,[64] rather peptide mimics can be candidates. Therefore, appropriate modification of the relatively nonessential residues of FOXO4 CR3 except for the four amino acids that were sensitive to the access of p53 DBD is recommended in the direction of drug development that interferes with PPIs of p53. α-Helix induction through leucine substitution could be a good example.[65] Moreover, introducing an additional FOXO4 CR3 sequence, which is important for p53 binding, next to the FOXO4 DRI peptide is expected to be a reasonable candidate for making more precise and specific p53 inhibitors.

bioRxiv preprint doi: https://doi.org/10.1101/2021.01.11.425814; this version posted January 11, 2021. The copyright holder for this preprint (which was not certified by peer review) is the author/funder, who has granted bioRxiv a license to display the preprint in perpetuity. It is made available under aCC-BY-NC-ND 4.0 International license.

Conclusions

Cellular senescence is a process that protects against unexpected oncogenic stress in somatic cells. However, the accumulation of senescent cells causes aging and diseases such as cancer. Understanding protein interactions involved in cellular senescence could provide a clue to elucidating its cause and overcoming disease through appropriate targeting. Through the study of the FOXO4-p53 axis, we observed that the FOXO4 and p53 interaction has dual binding surfaces, providing their DNA binding and transactivation domains as contact points. In addition, a model is presented for how the interaction of two TFs cooperates with the transcription initiation of a downstream gene. This study could provide essential structural information for drug development to overcome senescence-associated diseases.

bioRxiv preprint doi: https://doi.org/10.1101/2021.01.11.425814; this version posted January 11, 2021. The copyright holder for this preprint (which was not certified by peer review) is the author/funder, who has granted bioRxiv a license to display the preprint in perpetuity. It is made available under aCC-BY-NC-ND 4.0 International license.

Methods

Sample preparation

The full-length FOXO4 and p53 genes were acquired from Addgene. FOXO4 FHD (95-195) and p53 DBD (94-312) were subcloned into the pET His6 TEV LIC cloning vector (2B-T) (a gift from Scott Gradia, Addgene plasmid #29666) and transformed into *E. coli* BL21 (DE3) cells. FOXO4 CR3 (469-505) and p53 TAD (13-61) were subcloned into the pET His6 GST TEV LIC cloning vector (2G-T) (a gift from Scott Gradia, Addgene plasmid #29707) and transformed into *E. coli* BL21 (DE3) pLysS cells. All cells were grown at 37 °C to an OD_{600} of 0.7 in Luria-Bertani (LB) medium, and 0.5 mM of isopropyl-1-thio-β-D-galactopyranoside (IPTG) was added. Cells were cultured overnight (20 h) at 18 °C after additional induction. Overexpressed proteins were purified on a Ni-NTA column (GE Healthcare) followed by gel filtration chromatography using Hi-Load 16/600 superdex 200 pg and 75 pg (GE Healthcare) on AKTA pure and AKTA prime systems. The composition of the buffer solution was 20 mM HEPES (pH 7.0), 50 mM NaCl, 0.5 mM DTT. Glutathione-S-transferase (GST) tagged recombinant protein samples were cleaved by Tobacco Etch Virus (TEV) protease. The four FOXO4 CR3 variants (M476A, I487A, S488A, and M491A) were generated from the *FOXO4* gene by a site-directed mutagenesis strategy. ^{15}N-labeled protein samples for ^{1}H-^{15}N HSQC experiments were obtained by culturing cells in M9 minimal media containing ^{15}N-labeled NH_4Cl. They had the same overexpression and purification process as cells cultured in LB media.

Nuclear magnetic resonance experiments

A Bruker 900 MHz NMR spectrometer (KBSI, Ochang) and 600 MHz NMR spectrometer (GIST, Gwangju) with cryogenic probes were used to conduct NMR experiments. The buffer solution conditions for all experiments were set to 20 mM NaPi (pH 7.0), 50 mM NaCl, 2 mM DTT and the temperature was set to 25 °C. Data processing and analysis were performed using Topspin (Bruker) and NMRFAM-Sparky software programs.[66] The amide nitrogens and protons of FOXO4 FHD,[47] FOXO4 CR3,[48] and p53 DBD[55] have been assigned previously. The backbone assignments of p53 TAD were obtained by performing ^{1}H-^{15}N HSQC, HNCO, HNCACO, HNCACB, and CBCACONH experiments at a concentration of 1.0 mM. ^{1}H-^{15}N HSQC titration experiments were performed by adding 0 μM, 75 μM, 150 μM, 225 μM, and 300 μM unlabeled protein to ^{15}N-labeled samples of 300 μM. Average CSP values ($\Delta\delta_{avg}$) were calculated using the following equation:

$$\Delta\delta_{avg}=\sqrt{(\Delta\delta_H)^2+(\Delta\delta_N/5.88)^2}$$

$\Delta\delta_H$ and $\Delta\delta_N$ are the chemical shift changes of the amide proton and nitrogen, respectively.

bioRxiv preprint doi: https://doi.org/10.1101/2021.01.11.425814; this version posted January 11, 2021. The copyright holder for this preprint (which was not certified by peer review) is the author/funder, who has granted bioRxiv a license to display the preprint in perpetuity. It is made available under aCC-BY-NC-ND 4.0 International license.

Isothermal titration calorimetry analysis

ITC experiments were performed in 20 mM HEPES (pH 7.0), 50 mM NaCl, 0.5 mM DTT buffer solution using a Nano-ITC SV instrument (GIST, Gwangju). Titration was performed by adding 10 μL of 1000 μM protein via syringe injection into 100 μM protein in the cell (1000 μL) 25 times. The temperature in all experiments was 25 °C; the first injection (10 μL) was not used in the analysis. The time interval between injections was 300-350 sec, and the stirring speed was 350 rpm. Error values of the result were derived from the results of 3 replicate experiments. The thermodynamic data (stoichiometry (n), dissociation constant (K_d), enthalpy change (ΔH), and entropy change (ΔS)) were analyzed using the 'Independent model' fitting of the NanoAnalyze software (TA Instruments). The Gibbs free energy change (ΔG) was calculated by the following equation:

$$\Delta G = \Delta H - T\Delta S.$$

bioRxiv preprint doi: https://doi.org/10.1101/2021.01.11.425814; this version posted January 11, 2021. The copyright holder for this preprint (which was not certified by peer review) is the author/funder, who has granted bioRxiv a license to display the preprint in perpetuity. It is made available under aCC-BY-NC-ND 4.0 International license.

Acknowledgments

We thank the high-field NMR facility at the Korea Basic Science Institute (KBSI, Ochang) and GIST Central Research Facilities (GIST, Gwangju) for allowing us to use their NMR spectrometers. This work was supported by the National Research Foundation of Korea [grant 2018R1A2B6004388 to C.-J.P], which is funded by the Korean government (MSIT); by a GIST Research Institute grant funded by GIST in 2020; and by the KBSI under the R&D program [Project No.D39700] supervised by the Ministry of Science and ICT, Korea.

Author Contributions

J.K., D.A., and C.-J.P. designed the study; J.K. and D.A. prepared samples; J.K., D.A., and C.-J.P. planned and performed experiments; J.K., D.A., and C.-J.P. analyzed the data; J.K., D.A., and C.-J.P. wrote the paper. All authors have given approval to the final version of the manuscript.

Declaration of competing interests: none

bioRxiv preprint doi: https://doi.org/10.1101/2021.01.11.425814; this version posted January 11, 2021. The copyright holder for this preprint (which was not certified by peer review) is the author/funder, who has granted bioRxiv a license to display the preprint in perpetuity. It is made available under aCC-BY-NC-ND 4.0 International license.

References

1 Myatt, S. S. & Lam, E. W. The emerging roles of forkhead box (Fox) proteins in cancer. *Nature reviews. Cancer* **7**, 847-859, doi:10.1038/nrc2223 (2007).

2 Carter, M. E. & Brunet, A. FOXO transcription factors. *Current biology : CB* **17**, R113-114, doi:10.1016/j.cub.2007.01.008 (2007).

3 Accili, D. & Arden, K. C. FoxOs at the crossroads of cellular metabolism, differentiation, and transformation. *Cell* **117**, 421-426, doi:10.1016/s0092-8674(04)00452-0 (2004).

4 Barthel, A., Schmoll, D. & Unterman, T. G. FoxO proteins in insulin action and metabolism. *Trends in endocrinology and metabolism: TEM* **16**, 183-189, doi:10.1016/j.tem.2005.03.010 (2005).

5 Birkenkamp, K. U. & Coffer, P. J. Regulation of cell survival and proliferation by the FOXO (Forkhead box, class O) subfamily of Forkhead transcription factors. *Biochemical Society transactions* **31**, 292-297, doi:10.1042/bst0310292 (2003).

6 Essers, M. A. *et al.* FOXO transcription factor activation by oxidative stress mediated by the small GTPase Ral and JNK. *The EMBO journal* **23**, 4802-4812, doi:10.1038/sj.emboj.7600476 (2004).

7 de Keizer, P. L. *et al.* Activation of forkhead box O transcription factors by oncogenic BRAF promotes p21cip1-dependent senescence. *Cancer research* **70**, 8526-8536, doi:10.1158/0008-5472.Can-10-1563 (2010).

8 van den Berg, M. C. *et al.* The small GTPase RALA controls c-Jun N-terminal kinase-mediated FOXO activation by regulation of a JIP1 scaffold complex. *The Journal of biological chemistry* **288**, 21729-21741, doi:10.1074/jbc.M113.463885 (2013).

9 Nagaich, A. K. *et al.* p53-induced DNA bending and twisting: p53 tetramer binds on the outer side of a DNA loop and increases DNA twisting. *Proceedings of the National Academy of Sciences of the United States of America* **96**, 1875-1880, doi:10.1073/pnas.96.5.1875 (1999).

10 Brownawell, A. M., Kops, G. J., Macara, I. G. & Burgering, B. M. Inhibition of nuclear import by protein kinase B (Akt) regulates the subcellular distribution and activity of the forkhead transcription factor AFX. *Molecular and cellular biology* **21**, 3534-3546, doi:10.1128/mcb.21.10.3534-3546.2001 (2001).

11 Baar, M. P. *et al.* Targeted Apoptosis of Senescent Cells Restores Tissue Homeostasis in Response to Chemotoxicity and Aging. *Cell* **169**, 132-147.e116, doi:10.1016/j.cell.2017.02.031 (2017).

12 Coppé, J. P. *et al.* Senescence-associated secretory phenotypes reveal cell-nonautonomous functions of oncogenic RAS and the p53 tumor suppressor. *PLoS biology* **6**, 2853-2868, doi:10.1371/journal.pbio.0060301 (2008).

13 Rodier, F. *et al.* Persistent DNA damage signalling triggers senescence-associated inflammatory cytokine secretion. *Nature cell biology* **11**, 973-979, doi:10.1038/ncb1909 (2009).

14 McHugh, D. & Gil, J. Senescence and aging: Causes, consequences, and therapeutic avenues. *The Journal of cell biology* **217**, 65-77, doi:10.1083/jcb.201708092 (2018).

15 Rosso, A. *et al.* p53 Mediates the accelerated onset of senescence of endothelial progenitor cells in diabetes. *The Journal of biological chemistry* **281**, 4339-4347, doi:10.1074/jbc.M509293200 (2006).

16 Jeon, O. H. *et al.* Local clearance of senescent cells attenuates the development of post-traumatic osteoarthritis and creates a pro-regenerative environment. *Nature medicine* **23**, 775-781, doi:10.1038/nm.4324 (2017).

17 Gorgoulis, V. G. *et al.* p53-dependent ICAM-1 overexpression in senescent human cells identified in atherosclerotic lesions. *Laboratory investigation; a journal of technical methods and pathology* **85**, 502-511, doi:10.1038/labinvest.3700241 (2005).

18 Querfurth, H. W. & LaFerla, F. M. Alzheimer's disease. *The New England journal of medicine* **362**, 329-344, doi:10.1056/NEJMra0909142 (2010).

19 Bansal, R. & Nikiforov, M. A. Pathways of oncogene-induced senescence in human melanocytic cells. *Cell cycle (Georgetown, Tex.)* **9**, 2782-2788, doi:10.4161/cc.9.14.12551 (2010).

20 Klotz, L. O. *et al.* Redox regulation of FoxO transcription factors. *Redox biology* **6**, 51-72, doi:10.1016/j.redox.2015.06.019 (2015).

bioRxiv preprint doi: https://doi.org/10.1101/2021.01.11.425814; this version posted January 11, 2021. The copyright holder for this preprint (which was not certified by peer review) is the author/funder, who has granted bioRxiv a license to display the preprint in perpetuity. It is made available under aCC-BY-NC-ND 4.0 International license.

21 Biggs, W. H., 3rd, Cavenee, W. K. & Arden, K. C. Identification and characterization of members of the FKHR (FOX O) subclass of winged-helix transcription factors in the mouse. *Mammalian genome : official journal of the International Mammalian Genome Society* **12**, 416-425, doi:10.1007/s003350020002 (2001).

22 Furuyama, T., Nakazawa, T., Nakano, I. & Mori, N. Identification of the differential distribution patterns of mRNAs and consensus binding sequences for mouse DAF-16 homologues. *The Biochemical journal* **349**, 629-634, doi:10.1042/0264-6021:3490629 (2000).

23 Hartlmüller, C., Spreitzer, E., Göbl, C., Falsone, F. & Madl, T. NMR characterization of solvent accessibility and transient structure in intrinsically disordered proteins. *Journal of biomolecular NMR* **73**, 305-317, doi:10.1007/s10858-019-00248-2 (2019).

24 Shtutman, M., Chang, B. D., Schools, G. P. & Broude, E. V. Cellular Model of p21-Induced Senescence. *Methods in molecular biology (Clifton, N.J.)* **1534**, 31-39, doi:10.1007/978-1-4939-6670-7_3 (2017).

25 Kruiswijk, F., Labuschagne, C. F. & Vousden, K. H. p53 in survival, death and metabolic health: a lifeguard with a licence to kill. *Nature reviews. Molecular cell biology* **16**, 393-405, doi:10.1038/nrm4007 (2015).

26 Liu, G. *et al*. Chromosome stability, in the absence of apoptosis, is critical for suppression of tumorigenesis in Trp53 mutant mice. *Nature genetics* **36**, 63-68, doi:10.1038/ng1282 (2004).

27 Rowan, S. *et al*. Specific loss of apoptotic but not cell-cycle arrest function in a human tumor derived p53 mutant. *The EMBO journal* **15**, 827-838 (1996).

28 Toledo, F. *et al*. A mouse p53 mutant lacking the proline-rich domain rescues Mdm4 deficiency and provides insight into the Mdm2-Mdm4-p53 regulatory network. *Cancer cell* **9**, 273-285, doi:10.1016/j.ccr.2006.03.014 (2006).

29 Vousden, K. H. & Prives, C. Blinded by the Light: The Growing Complexity of p53. *Cell* **137**, 413-431, doi:10.1016/j.cell.2009.04.037 (2009).

30 Bourgeois, B. & Madl, T. Regulation of cellular senescence via the FOXO4-p53 axis. *FEBS letters* **592**, 2083-2097, doi:10.1002/1873-3468.13057 (2018).

31 Tran, H. *et al*. DNA repair pathway stimulated by the forkhead transcription factor FOXO3a through the Gadd45 protein. *Science (New York, N.Y.)* **296**, 530-534, doi:10.1126/science.1068712 (2002).

32 Seoane, J., Le, H. V., Shen, L., Anderson, S. A. & Massagué, J. Integration of Smad and forkhead pathways in the control of neuroepithelial and glioblastoma cell proliferation. *Cell* **117**, 211-223, doi:10.1016/s0092-8674(04)00298-3 (2004).

33 Miyauchi, H. *et al*. Akt negatively regulates the in vitro lifespan of human endothelial cells via a p53/p21-dependent pathway. *The EMBO journal* **23**, 212-220, doi:10.1038/sj.emboj.7600045 (2004).

34 Niculescu, A. B., 3rd *et al*. Effects of p21(Cip1/Waf1) at both the G1/S and the G2/M cell cycle transitions: pRb is a critical determinant in blocking DNA replication and in preventing endoreduplication. *Molecular and cellular biology* **18**, 629-643, doi:10.1128/mcb.18.1.629 (1998).

35 Chang, B. D. *et al*. Effects of p21Waf1/Cip1/Sdi1 on cellular gene expression: implications for carcinogenesis, senescence, and age-related diseases. *Proceedings of the National Academy of Sciences of the United States of America* **97**, 4291-4296, doi:10.1073/pnas.97.8.4291 (2000).

36 Mihara, M. *et al*. p53 has a direct apoptogenic role at the mitochondria. *Molecular cell* **11**, 577-590, doi:10.1016/s1097-2765(03)00050-9 (2003).

37 Wang, F. *et al*. Biochemical and structural characterization of an intramolecular interaction in FOXO3a and its binding with p53. *Journal of molecular biology* **384**, 590-603, doi:10.1016/j.jmb.2008.09.025 (2008).

38 Wang, F. *et al*. Structures of KIX domain of CBP in complex with two FOXO3a transactivation domains reveal promiscuity and plasticity in coactivator recruitment. *Proceedings of the National Academy of Sciences of the United States of America* **109**, 6078-6083, doi:10.1073/pnas.1119073109 (2012).

39 Lee, C. W., Martinez-Yamout, M. A., Dyson, H. J. & Wright, P. E. Structure of the p53 transactivation domain in complex with the nuclear receptor coactivator binding domain of CREB binding protein. *Biochemistry* **49**, 9964-9971, doi:10.1021/bi1012996 (2010).

bioRxiv preprint doi: https://doi.org/10.1101/2021.01.11.425814; this version posted January 11, 2021. The copyright holder for this preprint (which was not certified by peer review) is the author/funder, who has granted bioRxiv a license to display the preprint in perpetuity. It is made available under aCC-BY-NC-ND 4.0 International license.

40 Rowell, J. P., Simpson, K. L., Stott, K., Watson, M. & Thomas, J. O. HMGB1-facilitated p53 DNA binding occurs via HMG-Box/p53 transactivation domain interaction, regulated by the acidic tail. *Structure (London, England : 1993)* **20**, 2014-2024, doi:10.1016/j.str.2012.09.004 (2012).

41 Bochkareva, E. *et al.* Single-stranded DNA mimicry in the p53 transactivation domain interaction with replication protein A. *Proceedings of the National Academy of Sciences of the United States of America* **102**, 15412-15417, doi:10.1073/pnas.0504614102 (2005).

42 Chang, J., Kim, D. H., Lee, S. W., Choi, K. Y. & Sung, Y. C. Transactivation ability of p53 transcriptional activation domain is directly related to the binding affinity to TATA-binding protein. *The Journal of biological chemistry* **270**, 25014-25019, doi:10.1074/jbc.270.42.25014 (1995).

43 Chi, S. W. *et al.* Structural details on mdm2-p53 interaction. *The Journal of biological chemistry* **280**, 38795-38802, doi:10.1074/jbc.M508578200 (2005).

44 Kussie, P. H. *et al.* Structure of the MDM2 oncoprotein bound to the p53 tumor suppressor transactivation domain. *Science (New York, N.Y.)* **274**, 948-953, doi:10.1126/science.274.5289.948 (1996).

45 Feng, H. *et al.* Structural basis for p300 Taz2-p53 TAD1 binding and modulation by phosphorylation. *Structure (London, England : 1993)* **17**, 202-210, doi:10.1016/j.str.2008.12.009 (2009).

46 Follis, A. V. *et al.* The DNA-binding domain mediates both nuclear and cytosolic functions of p53. *Nature structural & molecular biology* **21**, 535-543, doi:10.1038/nsmb.2829 (2014).

47 Weigelt, J., Climent, I., Dahlman-Wright, K. & Wikström, M. 1H, 13C and 15N resonance assignments of the DNA binding domain of the human forkhead transcription factor AFX. *Journal of biomolecular NMR* **17**, 181-182, doi:10.1023/a:1008358816478 (2000).

48 Kim, J., Ahn, D., Park, C. J. FOXO4 transactivation domain interaction with forkhead DNA binding domain and effect on selective DNA recognition for transcription initiation. *Journal of molecular biology* **in press** (2021).

49 Brady, C. A. *et al.* Distinct p53 transcriptional programs dictate acute DNA-damage responses and tumor suppression. *Cell* **145**, 571-583, doi:10.1016/j.cell.2011.03.035 (2011).

50 Lee, M. S., Lim, K., Lee, M. K. & Chi, S. W. Structural Basis for the Interaction between p53 Transactivation Domain and the Mediator Subunit MED25. *Molecules (Basel, Switzerland)* **23**, doi:10.3390/molecules23102726 (2018).

51 Krois, A. S., Dyson, H. J. & Wright, P. E. Long-range regulation of p53 DNA binding by its intrinsically disordered N-terminal transactivation domain. *Proceedings of the National Academy of Sciences of the United States of America* **115**, E11302-e11310, doi:10.1073/pnas.1814051115 (2018).

52 el-Deiry, W. S., Kern, S. E., Pietenpol, J. A., Kinzler, K. W. & Vogelstein, B. Definition of a consensus binding site for p53. *Nature genetics* **1**, 45-49, doi:10.1038/ng0492-45 (1992).

53 Petros, A. M., Gunasekera, A., Xu, N., Olejniczak, E. T. & Fesik, S. W. Defining the p53 DNA-binding domain/Bcl-x(L)-binding interface using NMR. *FEBS letters* **559**, 171-174, doi:10.1016/s0014-5793(04)00059-6 (2004).

54 Rudiger, S., Freund, S. M., Veprintsev, D. B. & Fersht, A. R. CRINEPT-TROSY NMR reveals p53 core domain bound in an unfolded form to the chaperone Hsp90. *Proceedings of the National Academy of Sciences of the United States of America* **99**, 11085-11090, doi:10.1073/pnas.132393699 (2002).

55 Wong, K. B. *et al.* Hot-spot mutants of p53 core domain evince characteristic local structural changes. *Proceedings of the National Academy of Sciences of the United States of America* **96**, 8438-8442, doi:10.1073/pnas.96.15.8438 (1999).

56 Cañadillas, J. M. *et al.* Solution structure of p53 core domain: structural basis for its instability. *Proceedings of the National Academy of Sciences of the United States of America* **103**, 2109-2114, doi:10.1073/pnas.0510941103 (2006).

57 Petty, T. J. *et al.* An induced fit mechanism regulates p53 DNA binding kinetics to confer sequence specificity. *The EMBO journal* **30**, 2167-2176, doi:10.1038/emboj.2011.127 (2011).

58 Chène, P. Inhibiting the p53-MDM2 interaction: an important target for cancer therapy. *Nature reviews. Cancer* **3**, 102-109, doi:10.1038/nrc991 (2003).

59 Chien, P. & Gierasch, L. M. Challenges and dreams: physics of weak interactions essential to life. *Molecular biology of the cell* **25**, 3474-3477, doi:10.1091/mbc.E14-06-1035 (2014).

bioRxiv preprint doi: https://doi.org/10.1101/2021.01.11.425814; this version posted January 11, 2021. The copyright holder for this preprint (which was not certified by peer review) is the author/funder, who has granted bioRxiv a license to display the preprint in perpetuity. It is made available under aCC-BY-NC-ND 4.0 International license.

60 Rabouille, C. & Alberti, S. Cell adaptation upon stress: the emerging role of membrane-less compartments. *Current opinion in cell biology* **47**, 34-42, doi:10.1016/j.ceb.2017.02.006 (2017).

61 Sukenik, S., Ren, P. & Gruebele, M. Weak protein-protein interactions in live cells are quantified by cell-volume modulation. *Proceedings of the National Academy of Sciences of the United States of America* **114**, 6776-6781, doi:10.1073/pnas.1700818114 (2017).

62 Hernandez-Munain, C., Roberts, J. L. & Krangel, M. S. Cooperation among multiple transcription factors is required for access to minimal T-cell receptor alpha-enhancer chromatin in vivo. *Molecular and cellular biology* **18**, 3223-3233, doi:10.1128/mcb.18.6.3223 (1998).

63 Nie, Y., Shu, C. & Sun, X. Cooperative binding of transcription factors in the human genome. *Genomics* **112**, 3427-3434, doi:10.1016/j.ygeno.2020.06.029 (2020).

64 Calissi, G., Lam, E. W. & Link, W. Therapeutic strategies targeting FOXO transcription factors. *Nature reviews. Drug discovery*, doi:10.1038/s41573-020-0088-2 (2020).

65 Langlois, C. *et al*. Structure-based design of a potent artificial transactivation domain based on p53. *Journal of the American Chemical Society* **134**, 1715-1723, doi:10.1021/ja208999e (2012).

66 Lee, W., Tonelli, M. & Markley, J. L. NMRFAM-SPARKY: enhanced software for biomolecular NMR spectroscopy. *Bioinformatics (Oxford, England)* **31**, 1325-1327, doi:10.1093/bioinformatics/btu830 (2015).

bioRxiv preprint doi: https://doi.org/10.1101/2021.01.11.425814; this version posted January 11, 2021. The copyright holder for this preprint (which was not certified by peer review) is the author/funder, who has granted bioRxiv a license to display the preprint in perpetuity. It is made available under aCC-BY-NC-ND 4.0 International license.

Figure captions

Figure 1. Domain structure of (A) FOXO4 and (B) p53. The primary sequences of FOXO4 FHD and CR3 and p53 TAD and DBD are shown as expansions indicated by arrows.

Figure 2. Chemical shift changes of FOXO4 FHD upon titration with p53 domains. (A-B) Overlaid ^{1}H-^{15}N HSQC spectra of ^{15}N-labeled FOXO4 FHD at a concentration of 300 μM with increasing concentrations (0 μM, 75 μM, 150 μM, 225 μM, 300 μM) of (A) p53 TAD and (B) p53 DBD. (C-D) $\Delta\delta_{avg}$ for each FOXO4 FHD residue when (C) p53 TAD and (D) p53 DBD concentrations are 300 μM, respectively. (E) The solution structure of FOXO4 FHD (PDB ID: 1E17),[47] colored based on CSP data with p53 TAD. Residues that undergo a large chemical shift change are colored in red (above average + 2σ) and blue (above average + 1σ). Basic amino acids of FOXO4 FHD are colored in cyan.

Figure 3. Chemical shift changes of p53 domains upon titration with FOXO4 FHD. (A) Overlaid ^{1}H-^{15}N HSQC spectra of 300 μM of (A) ^{15}N-labeled p53 TAD and (B) ^{15}N-labeled p53 DBD with increasing concentrations (0 μM, 75 μM, 150 μM, 225 μM, 300 μM) of FOXO4 FHD. (C-D) $\Delta\delta_{avg}$ for each (C) p53 TAD and (D) p53 DBD residue when FOXO4 FHD concentration is 300 μM, respectively. Residues that undergo a large chemical shift change are colored in red (above average + 2σ) and blue (above average + 1σ).

Figure 4. Chemical shift changes of FOXO4 CR3 upon titration with p53 DBD. (A) Overlaid ^{1}H-^{15}N HSQC spectra of ^{15}N-labeled FOXO4 CR3 at a concentration of 300 μM with increasing concentrations (0 μM, 75 μM, 150 μM, 225 μM, 300 μM) of p53 DBD. (B) $\Delta\delta_{avg}$ for each FOXO4 CR3 residue when p53 DBD concentration is 300 μM. Residues that undergo a large chemical shift change are colored in red (above average + 1σ) and blue (above average).

Figure 5. Chemical shift changes of p53 DBD upon titration with FOXO4 CR3. (A) Overlaid ^{1}H-^{15}N HSQC spectra of ^{15}N-labeled p53 DBD at a concentration of 300 μM with increasing concentrations (0 μM, 75 μM, 150 μM, 225 μM, 300 μM) of FOXO4 CR3. (B) $\Delta\delta_{avg}$ for each p53 DBD residue when FOXO4 CR3 concentration is 300 μM. (C) The solution structure of p53 DBD (PDB ID: 2FEJ),[56] colored based on CSP data with FOXO4 CR3. (D) The solution structure of p53 DBD with DNA (PDB ID: 3Q05).[57] Residues that undergo a large chemical shift change are colored in red (above average + 2σ) and pink (above average + 1σ). Residues that participate only in DNA binding are colored in cyan, and those involved in the binding of both DNA and FOXO4 CR3 are shown in blue.

Figure 6. Chemical shift changes of p53 DBD after titration with FOXO4 CR3 alanine mutants. $\Delta\delta_{avg}$ for each ^{15}N-labeled p53 DBD at a concentration of 300 μM when concentration of FOXO4 CR3 (A) M476A, (B) I487A, (C) S488A, and (D) M491A are 300 μM (left column). Residues that undergo a

bioRxiv preprint doi: https://doi.org/10.1101/2021.01.11.425814; this version posted January 11, 2021. The copyright holder for this preprint (which was not certified by peer review) is the author/funder, who has granted bioRxiv a license to display the preprint in perpetuity. It is made available under aCC-BY-NC-ND 4.0 International license.

large chemical shift change in ^{15}N-labeled p53 DBD and FOXO4 CR3 titration are colored in red (above average + 2σ) and pink (above average + 1σ). Vertical pink bands indicate the regions between β-strands S2 and S3, and α-helix H3 of p53 DBD, which showed large perturbations in FOXO4 CR3 titration. The solution structure of p53 DBD (PDB ID: 2FEJ),[56] colored based on CSP data with FOXO4 CR3 alanine mutants (right column). Residues that undergo significant changes in both CR3 and its mutants are colored in red, and residues that undergo large perturbation in CR3 but reduced by mutation are colored in black.

Figure 7. Thermodynamic analysis of FOXO4-p53 domain interactions by ITC. Raw data of heat plot (upper panel) and integration plot of data (lower panel) when (A) FOXO4 FHD was injected into p53 TAD and (C) FOXO4 CR3 into p53 DBD. Binding affinity (K_d) and stoichiometry (n) between the two molecules in each sample are presented. Three thermodynamic parameters (ΔH, enthalpy change; ΔG, Gibbs energy of association; -TΔS, entropy change in temperature) of (B) FOXO4 FHD-p53 TAD interaction and (D) FOXO4 CR3-p53 DBD interaction obtained from the curve.

Figure 8. Model for cooperative transcription initiation of FOXO4 and p53.

bioRxiv preprint doi: https://doi.org/10.1101/2021.01.11.425814; this version posted January 11, 2021. The copyright holder for this preprint (which was not certified by peer review) is the author/funder, who has granted bioRxiv a license to display the preprint in perpetuity. It is made available under aCC-BY-NC-ND 4.0 International license.

Figures

Figure 1.

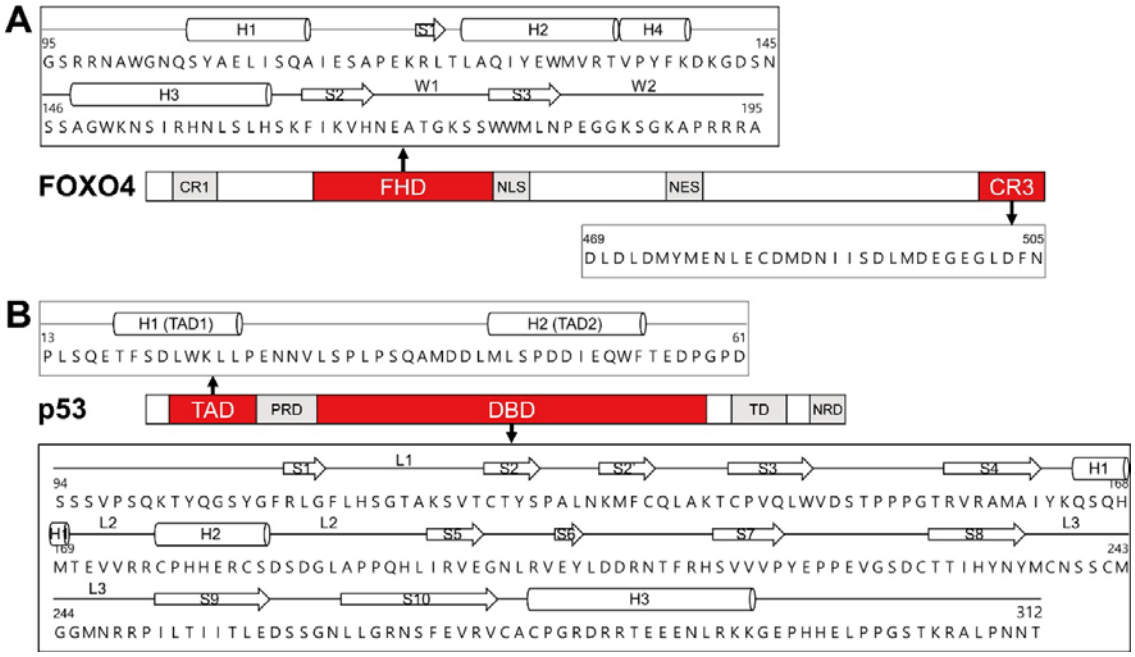

Figure 1. Domain structure of (A) FOXO4 and (B) p53. The primary sequences of FOXO4 FHD and CR3 and p53 TAD and DBD are shown as expansions indicated by arrows.

bioRxiv preprint doi: https://doi.org/10.1101/2021.01.11.425814; this version posted January 11, 2021. The copyright holder for this preprint (which was not certified by peer review) is the author/funder, who has granted bioRxiv a license to display the preprint in perpetuity. It is made available under aCC-BY-NC-ND 4.0 International license.

Figure 2.

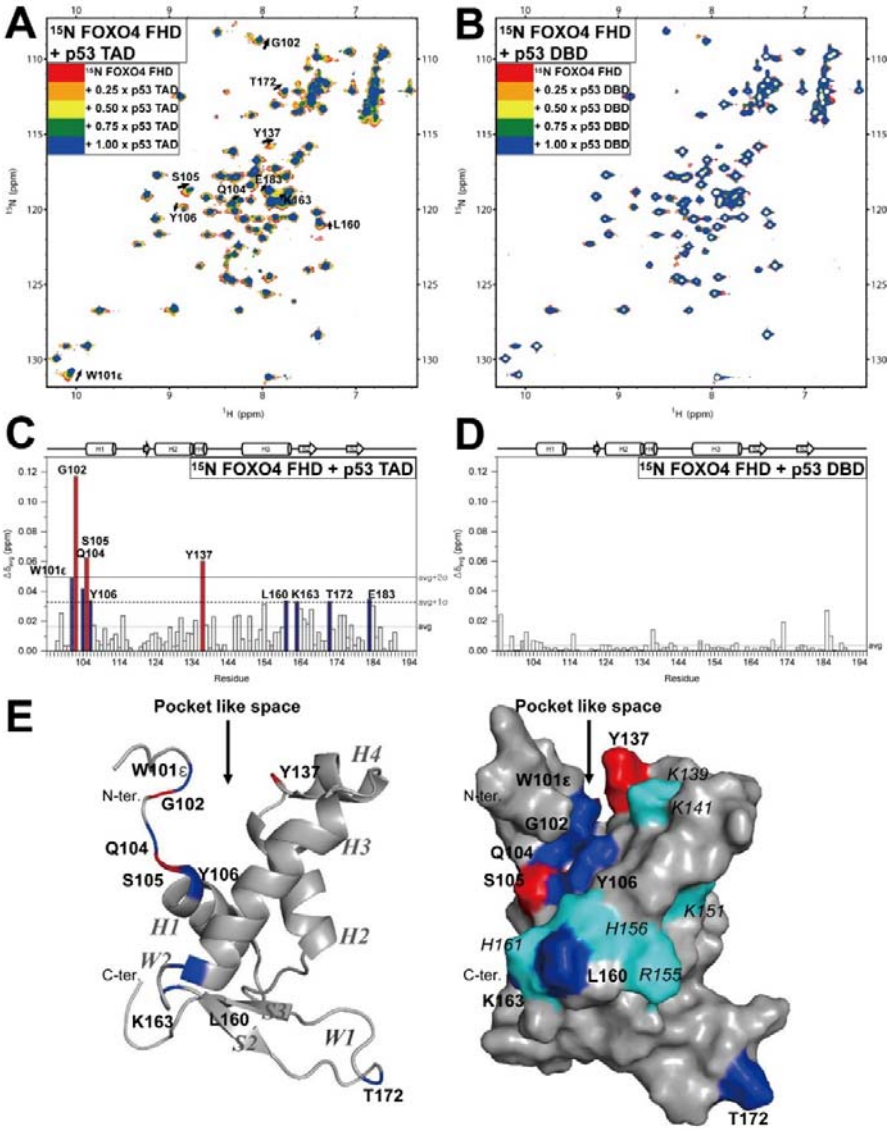

Figure 2. Chemical shift changes of FOXO4 FHD upon titration with p53 domains. (A-B) Overlaid ^{1}H-^{15}N HSQC spectra of ^{15}N-labeled FOXO4 FHD at a concentration of 300 μM with increasing concentrations (0 μM, 75 μM, 150 μM, 225 μM, 300 μM) of (A) p53 TAD and (B) p53 DBD. (C-D) $\Delta\delta_{avg}$ for each FOXO4 FHD residue when (C) p53 TAD and (D) p53 DBD concentrations are 300 μM, respectively. (E) The solution structure of FOXO4 FHD (PDB ID: 1E17),[47] colored based on CSP data with p53 TAD. Residues that undergo a large chemical shift change are colored in red (above average + 2σ) and blue (above average + 1σ). Basic amino acids of FOXO4 FHD are colored in cyan.

bioRxiv preprint doi: https://doi.org/10.1101/2021.01.11.425814; this version posted January 11, 2021. The copyright holder for this preprint (which was not certified by peer review) is the author/funder, who has granted bioRxiv a license to display the preprint in perpetuity. It is made available under aCC-BY-NC-ND 4.0 International license.

Figure 3.

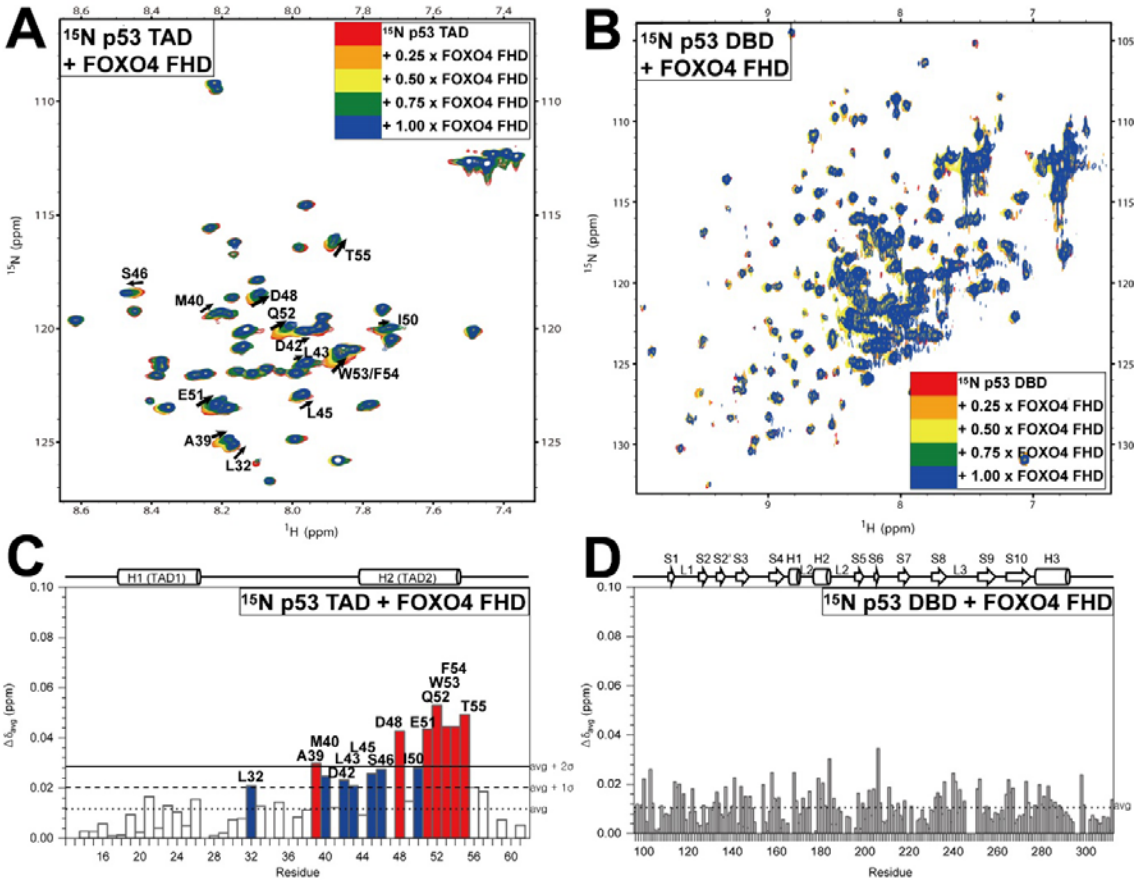

Figure 3. Chemical shift changes of p53 domains upon titration with FOXO4 FHD. (A) Overlaid ^{1}H-^{15}N HSQC spectra of 300 μM of (A) ^{15}N-labeled p53 TAD and (B) ^{15}N-labeled p53 DBD with increasing concentrations (0 μM, 75 μM, 150 μM, 225 μM, 300 μM) of FOXO4 FHD. (C-D) $\Delta\delta_{avg}$ for each (C) p53 TAD and (D) p53 DBD residue when FOXO4 FHD concentration is 300 μM, respectively. Residues that undergo a large chemical shift change are colored in red (above average + 2σ) and blue (above average + 1σ).

bioRxiv preprint doi: https://doi.org/10.1101/2021.01.11.425814; this version posted January 11, 2021. The copyright holder for this preprint (which was not certified by peer review) is the author/funder, who has granted bioRxiv a license to display the preprint in perpetuity. It is made available under aCC-BY-NC-ND 4.0 International license.

Figure 4.

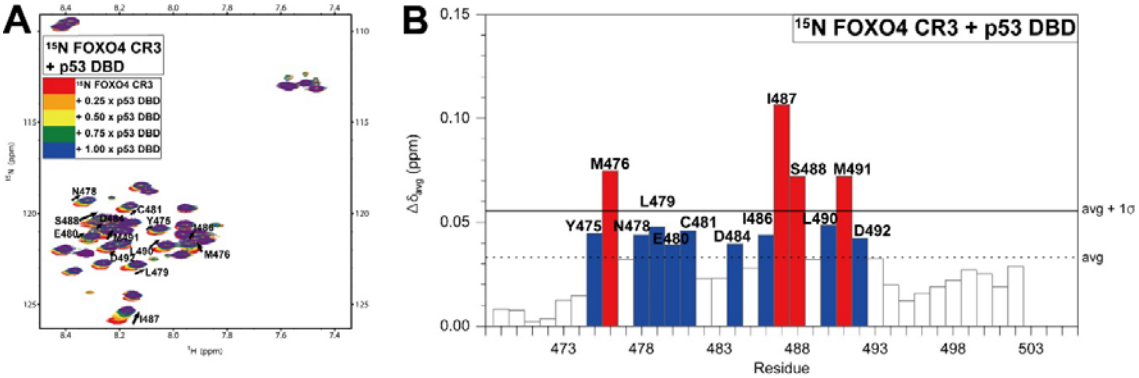

Figure 4. Chemical shift changes of FOXO4 CR3 upon titration with p53 DBD. (A) Overlaid ^{1}H-^{15}N HSQC spectra of ^{15}N-labeled FOXO4 CR3 at a concentration of 300 μM with increasing concentrations (0 μM, 75 μM, 150 μM, 225 μM, 300 μM) of p53 DBD. (B) $\Delta\delta_{avg}$ for each FOXO4 CR3 residue when p53 DBD concentration is 300 μM. Residues that undergo a large chemical shift change are colored in red (above average + 1σ) and blue (above average).

bioRxiv preprint doi: https://doi.org/10.1101/2021.01.11.425814; this version posted January 11, 2021. The copyright holder for this preprint (which was not certified by peer review) is the author/funder, who has granted bioRxiv a license to display the preprint in perpetuity. It is made available under aCC-BY-NC-ND 4.0 International license.

Figure 5.

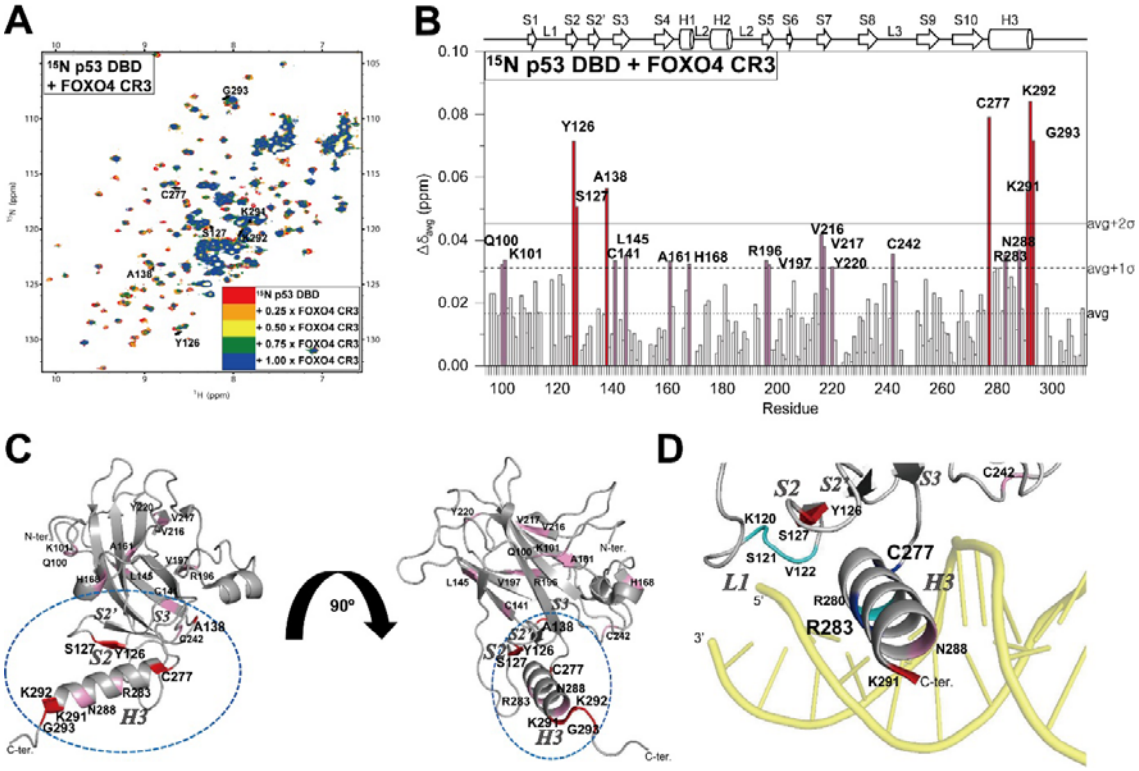

Figure 5. Chemical shift changes of p53 DBD upon titration with FOXO4 CR3. (A) Overlaid ^{1}H-^{15}N HSQC spectra of ^{15}N-labeled p53 DBD at a concentration of 300 μM with increasing concentrations (0 μM, 75 μM, 150 μM, 225 μM, 300 μM) of FOXO4 CR3. (B) $\Delta\delta_{avg}$ for each p53 DBD residue when FOXO4 CR3 concentration is 300 μM. (C) The solution structure of p53 DBD (PDB ID: 2FEJ),[56] colored based on CSP data with FOXO4 CR3. (D) The solution structure of p53 DBD with DNA (PDB ID: 3Q05).[57] Residues that undergo a large chemical shift change are colored in red (above average + 2σ) and pink (above average + 1σ). Residues that participate only in DNA binding are colored in cyan, and those involved in the binding of both DNA and FOXO4 CR3 are shown in blue.

bioRxiv preprint doi: https://doi.org/10.1101/2021.01.11.425814; this version posted January 11, 2021. The copyright holder for this preprint (which was not certified by peer review) is the author/funder, who has granted bioRxiv a license to display the preprint in perpetuity. It is made available under aCC-BY-NC-ND 4.0 International license.

Figure 6.

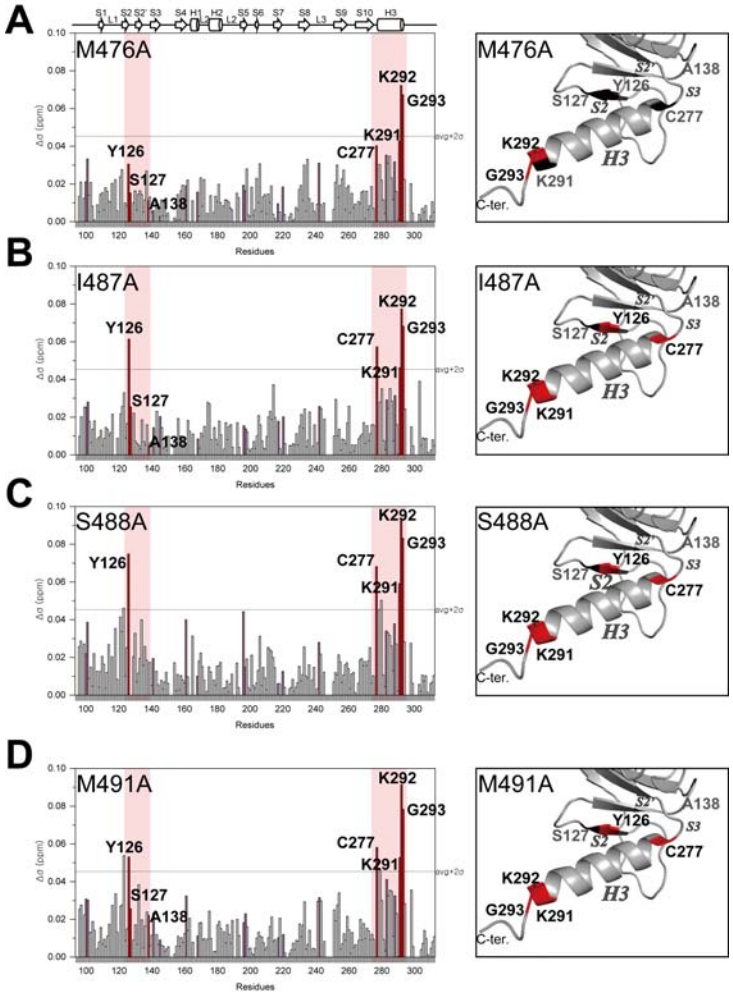

Figure 6. Chemical shift changes of p53 DBD after titration with FOXO4 CR3 alanine mutants. $\Delta\delta_{avg}$ for each ^{15}N-labeled p53 DBD at a concentration of 300 μM when concentration of FOXO4 CR3 (A) M476A, (B) I487A, (C) S488A, and (D) M491A are 300 μM (left column). Residues that undergo a large chemical shift change in ^{15}N-labeled p53 DBD and FOXO4 CR3 titration are colored in red (above average + 2σ) and pink (above average + 1σ). Vertical pink bands indicate the regions between β-strands S2 and S3, and α-helix H3 of p53 DBD, which showed large perturbations in FOXO4 CR3 titration. The solution structure of p53 DBD (PDB ID: 2FEJ),[56] colored based on CSP data with FOXO4 CR3 alanine mutants (right column). Residues that undergo significant changes in both CR3 and its mutants are colored in red, and residues that undergo large perturbation in CR3 but reduced by mutation are colored in black.

bioRxiv preprint doi: https://doi.org/10.1101/2021.01.11.425814; this version posted January 11, 2021. The copyright holder for this preprint (which was not certified by peer review) is the author/funder, who has granted bioRxiv a license to display the preprint in perpetuity. It is made available under aCC-BY-NC-ND 4.0 International license.

Figure 7.

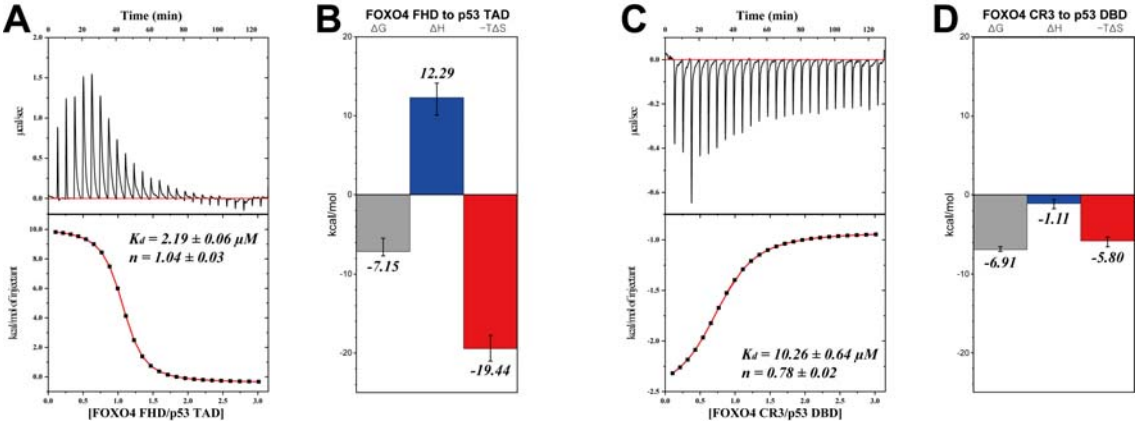

Figure 7. Thermodynamic analysis of FOXO4-p53 domain interactions by ITC. Raw data of heat plot (upper panel) and integration plot of data (lower panel) when (A) FOXO4 FHD was injected into p53 TAD and (C) FOXO4 CR3 into p53 DBD. Binding affinity (K_d) and stoichiometry (n) between the two molecules in each sample are presented. Three thermodynamic parameters (ΔH, enthalpy change; ΔG, Gibbs energy of association; -TΔS, entropy change in temperature) of (B) FOXO4 FHD-p53 TAD interaction and (D) FOXO4 CR3-p53 DBD interaction obtained from the curve.

bioRxiv preprint doi: https://doi.org/10.1101/2021.01.11.425814; this version posted January 11, 2021. The copyright holder for this preprint (which was not certified by peer review) is the author/funder, who has granted bioRxiv a license to display the preprint in perpetuity. It is made available under aCC-BY-NC-ND 4.0 International license.

Figure 8.

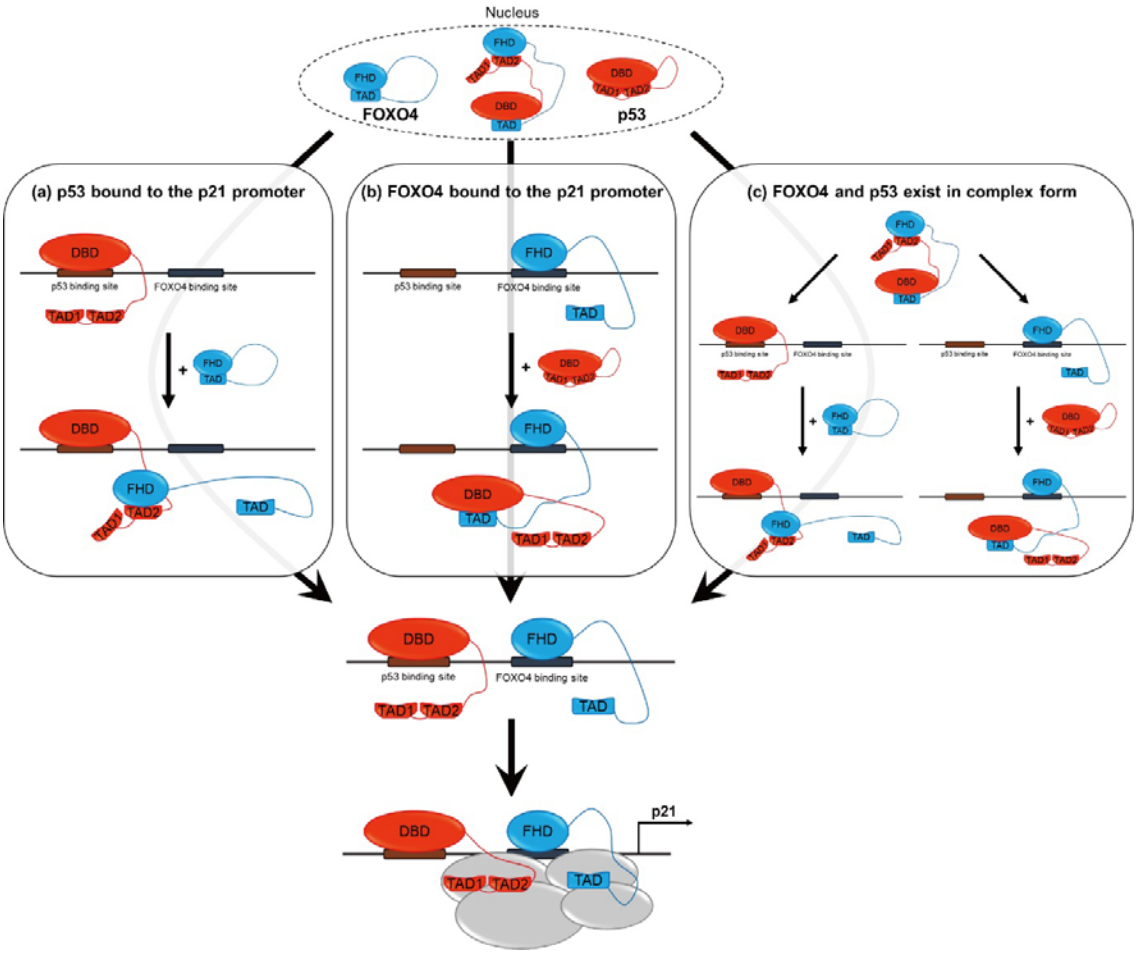

Figure 8. Model for cooperative transcription initiation of FOXO4 and p53.

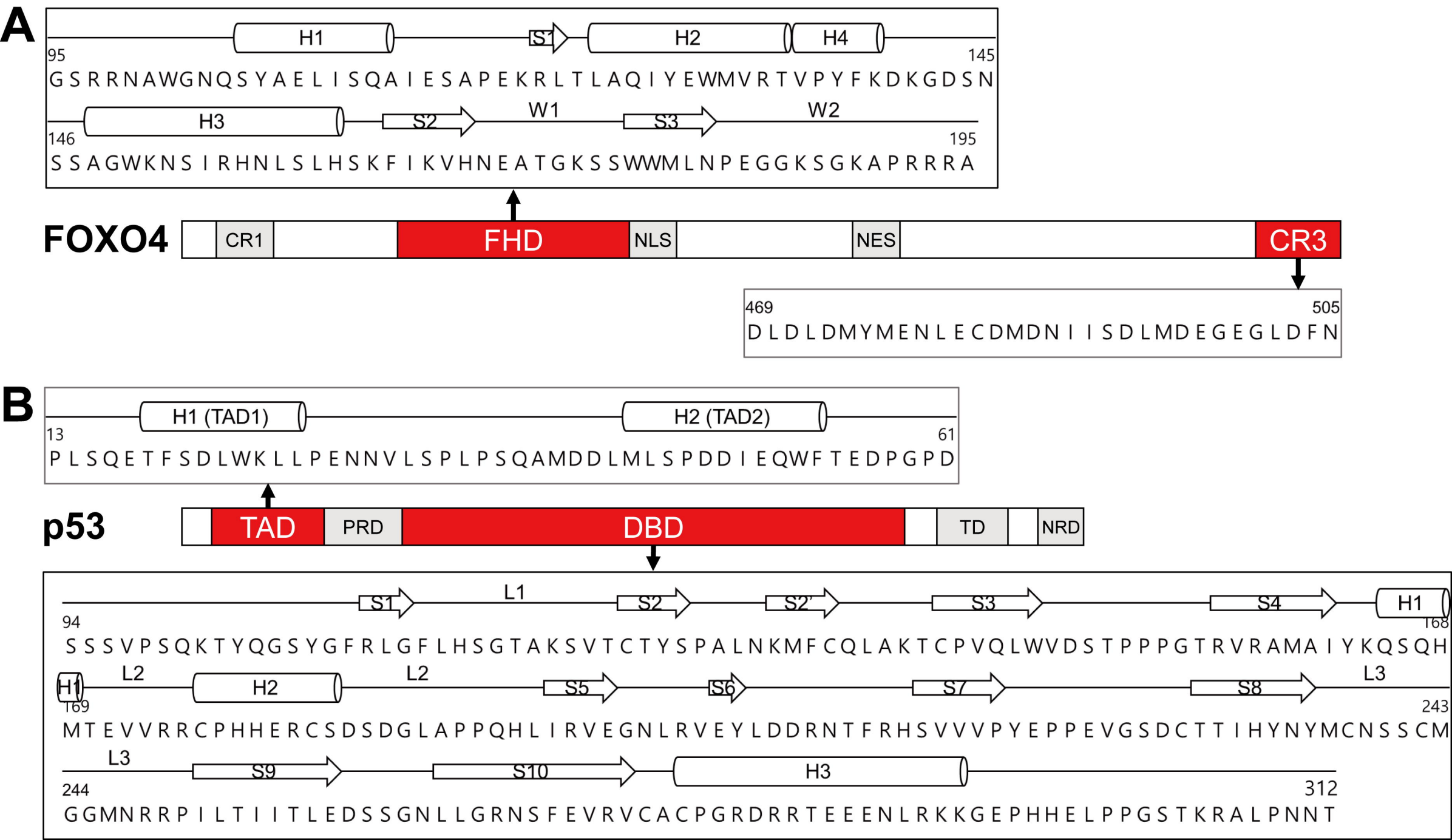
A
H1
S1
H2
H4
95
145
G S R R N A W G N Q S Y A E L I S Q A I E S A P E K R L T L A Q I Y E W M V R T V P Y F K D K G D S N
H3
S2
W1
S3
W2
146
195
S S A G W K N S I R H N L S L H S K F I K V H N E A T G K S S W W M L N P E G G K S G K A P R R R A
FOXO4
CR1
FHD
NLS
NES
CR3
469
505
D L D L D M Y M E N L E C D M D N I I S D L M D E G E G L D F N
B
H1 (TAD1)
H2 (TAD2)
13
61
P L S Q E T F S D L W K L L P E N N V L S P L P S Q A M D D L M L S P D D I E Q W F T E D P G P D
p53
TAD
PRD
DBD
TD
NRD
S1
L1
S2
S2'
S3
S4
H1
94
168
S S S V P S Q K T Y Q G S Y G F R L G F L H S G T A K S V T C T Y S P A L N K M F C Q L A K T C P V Q L W V D S T P P P G T R V R A M A I Y K Q S Q H
H1
L2
H2
L2
S5
S6
S7
S8
L3
169
243
M T E V V R R C P H H E R C S D S D G L A P P Q H L I R V E G N L R V E Y L D D R N T F R H S V V V P Y E P P E V G S D C T T I H Y N Y M C N S S C M
L3
S9
S10
H3
244
312
G G M N R R P I L T I I T L E D S S G N L L G R N S F E V R V C A C P G R D R R T E E E N L R K K G E P H H E L P P G S T K R A L P N N T

available under aCC-BY-NC-ND 4.0 International license.

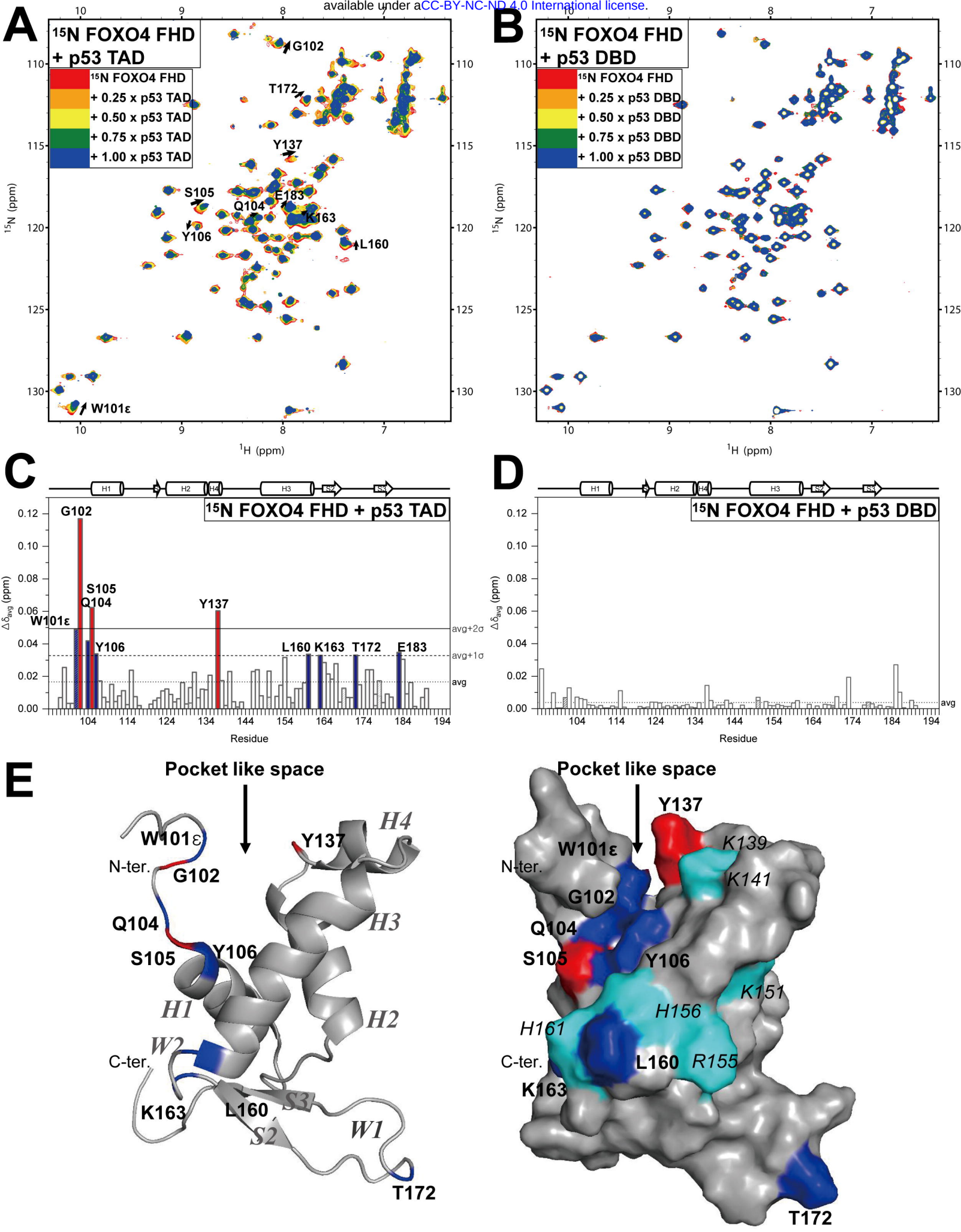

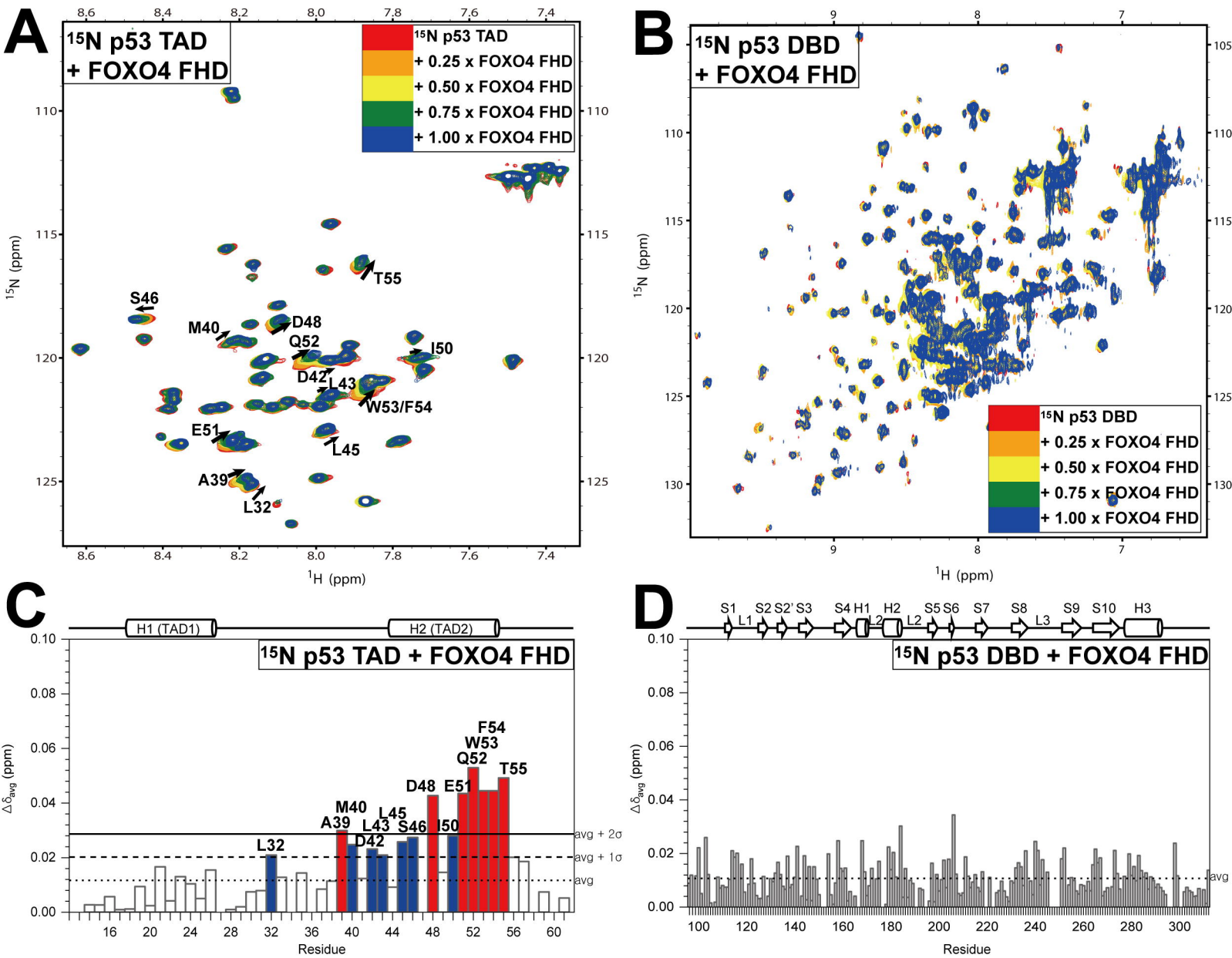
A
15N p53 TAD
+ FOXO4 FHD
15N p53 TAD
+ 0.25 x FOXO4 FHD
+ 0.50 x FOXO4 FHD
+ 0.75 x FOXO4 FHD
+ 1.00 x FOXO4 FHD
S46
M40
D48
Q52
T55
I50
D42
L43
W53/F54
E51
L45
A39
L32
15N (ppm)
1H (ppm)
B
15N p53 DBD
+ FOXO4 FHD
15N p53 DBD
+ 0.25 x FOXO4 FHD
+ 0.50 x FOXO4 FHD
+ 0.75 x FOXO4 FHD
+ 1.00 x FOXO4 FHD
15N (ppm)
1H (ppm)
C
H1 (TAD1)
H2 (TAD2)
15N p53 TAD + FOXO4 FHD
F54
W53
Q52
T55
D48
E51
M40
A39
L45
L43
S46
I50
D42
L32
avg + 2σ
avg + 1σ
avg
Δδavg (ppm)
Residue
D
S1 S2 S2' S3 S4 H1 H2 S5 S6 S7 S8 S9 S10 H3
L1 L2 L2 L3
15N p53 DBD + FOXO4 FHD
avg
Δδavg (ppm)
Residue

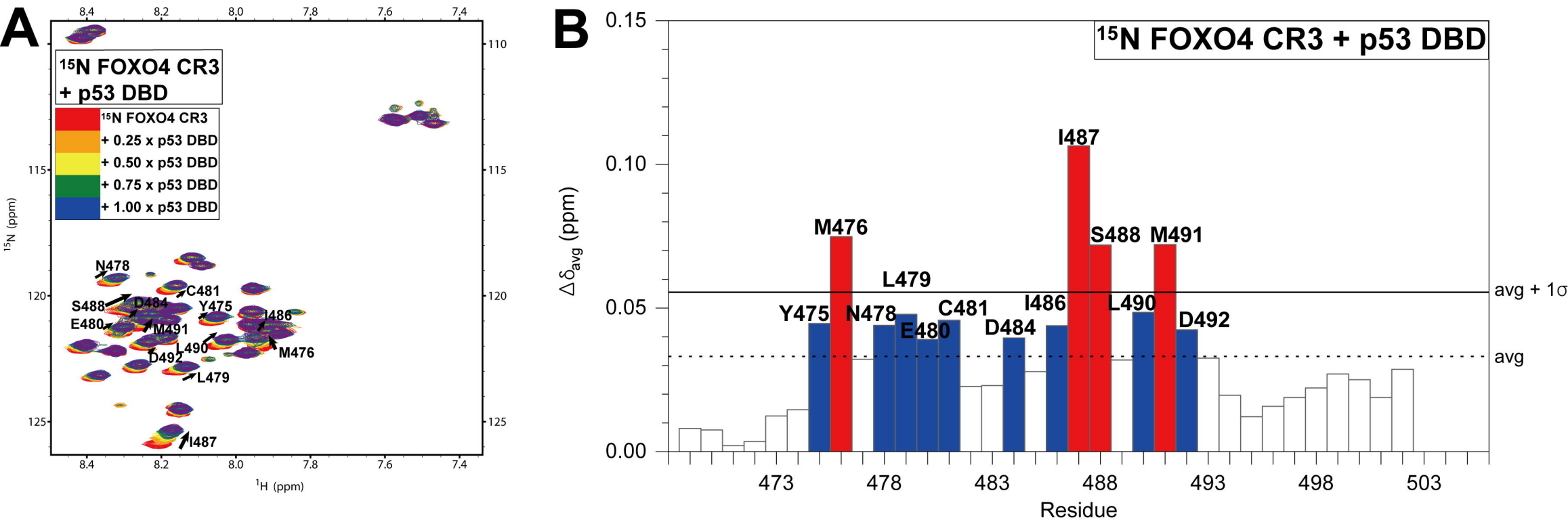
A
15N FOXO4 CR3 + p53 DBD
15N FOXO4 CR3
+ 0.25 x p53 DBD
+ 0.50 x p53 DBD
+ 0.75 x p53 DBD
+ 1.00 x p53 DBD
N478
C481
S488
D484
Y475
E480
M491
I486
L490
M476
D492
L479
I487
15N (ppm)
1H (ppm)
B
15N FOXO4 CR3 + p53 DBD
Δδavg (ppm)
avg + 1σ
avg
Residue
M476
L479
Y475
N478
E480
C481
D484
I487
I486
S488
L490
M491
D492

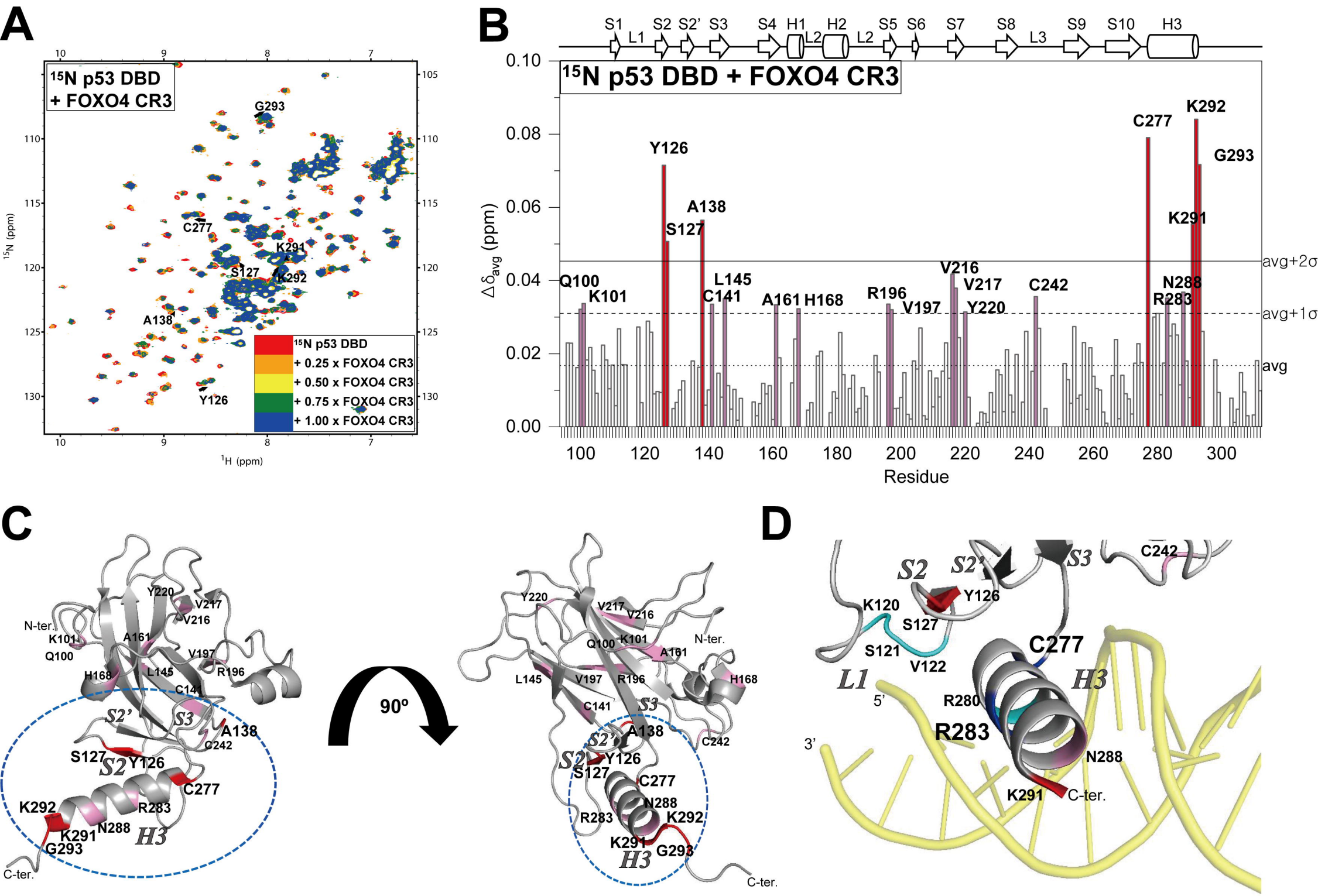
A
15N p53 DBD
+ FOXO4 CR3
G293
C277
K291
S127
K292
A138
Y126
15N p53 DBD
+ 0.25 x FOXO4 CR3
+ 0.50 x FOXO4 CR3
+ 0.75 x FOXO4 CR3
+ 1.00 x FOXO4 CR3
15N (ppm)
1H (ppm)
B
S1 L1 S2 S2' S3 S4 H1 L2 H2 L2 S5 S6 S7 S8 L3 S9 S10 H3
15N p53 DBD + FOXO4 CR3
Δδavg (ppm)
Q100
K101
Y126
A138
S127
L145
C141
A161
H168
R196
V197
V216
V217
Y220
C242
C277
K292
G293
K291
N288
R283
avg+2σ
avg+1σ
avg
Residue
C
N-ter.
Y220
V217
V216
K101
Q100
A161
V197
R196
H168
L145
C141
S2'
S3
A138
C242
S127
S2
Y126
C277
K292
R283
K291
N288
H3
G293
C-ter.
90°
Y220
V217
V216
Q100
K101
A161
N-ter.
L145
V197
R196
H168
C141
S3
S2'
A138
C242
S2
Y126
S127
C277
N288
R283
K292
K291
G293
H3
C-ter.
D
S2
S2'
S3
C242
Y126
K120
S127
S121
V122
C277
L1
H3
5'
R280
R283
3'
N288
K291
C-ter.

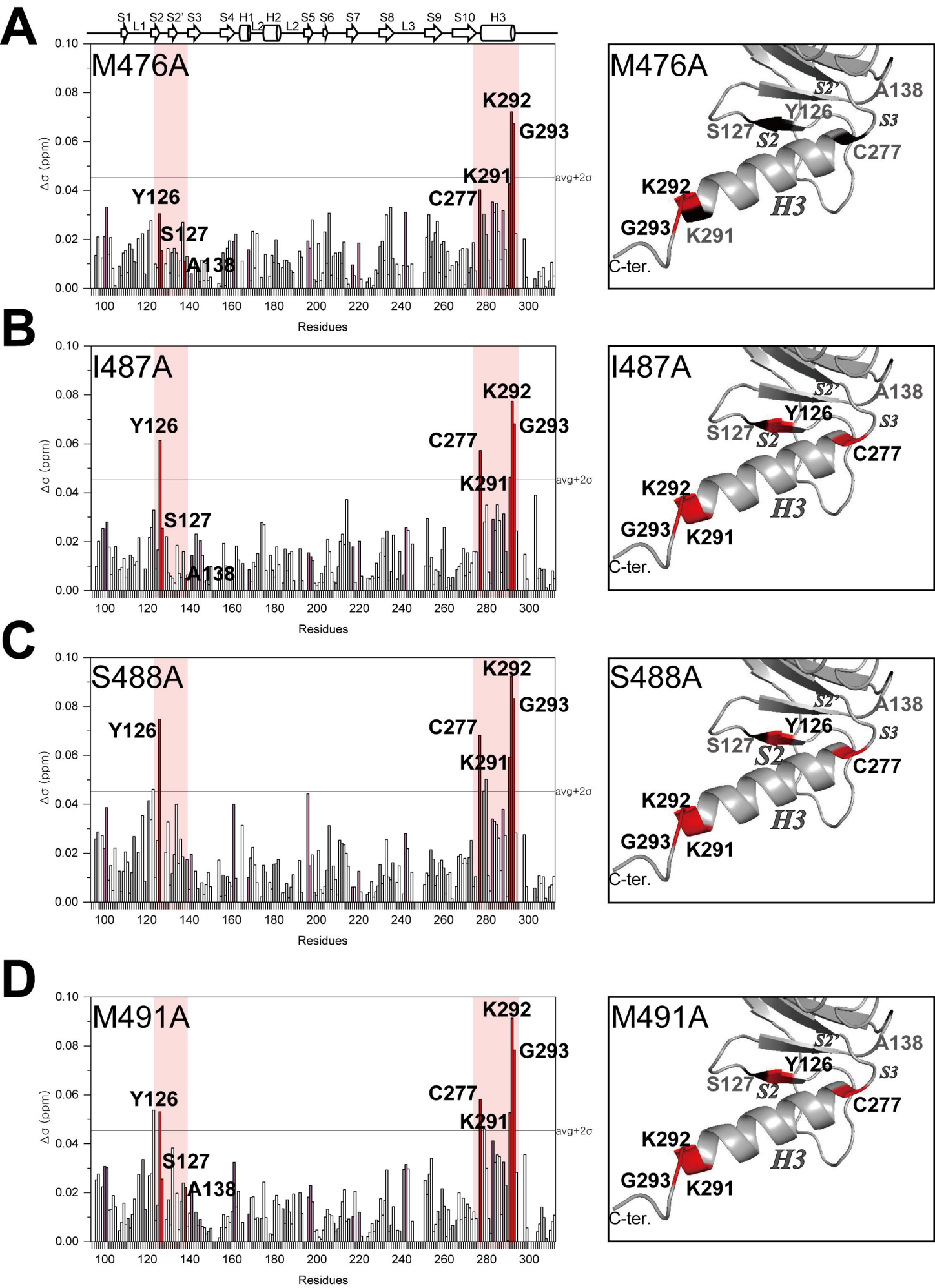
A
S1 L1 S2 S2' S3 S4 H1 L2 H2 L2 S5 S6 S7 S8 L3 S9 S10 H3
M476A
Δσ (ppm)
Residues
avg+2σ
Y126
S127
A138
C277
K291
K292
G293
S2'
S2
S3
H3
C-ter.
B
I487A
C
S488A
D
M491A

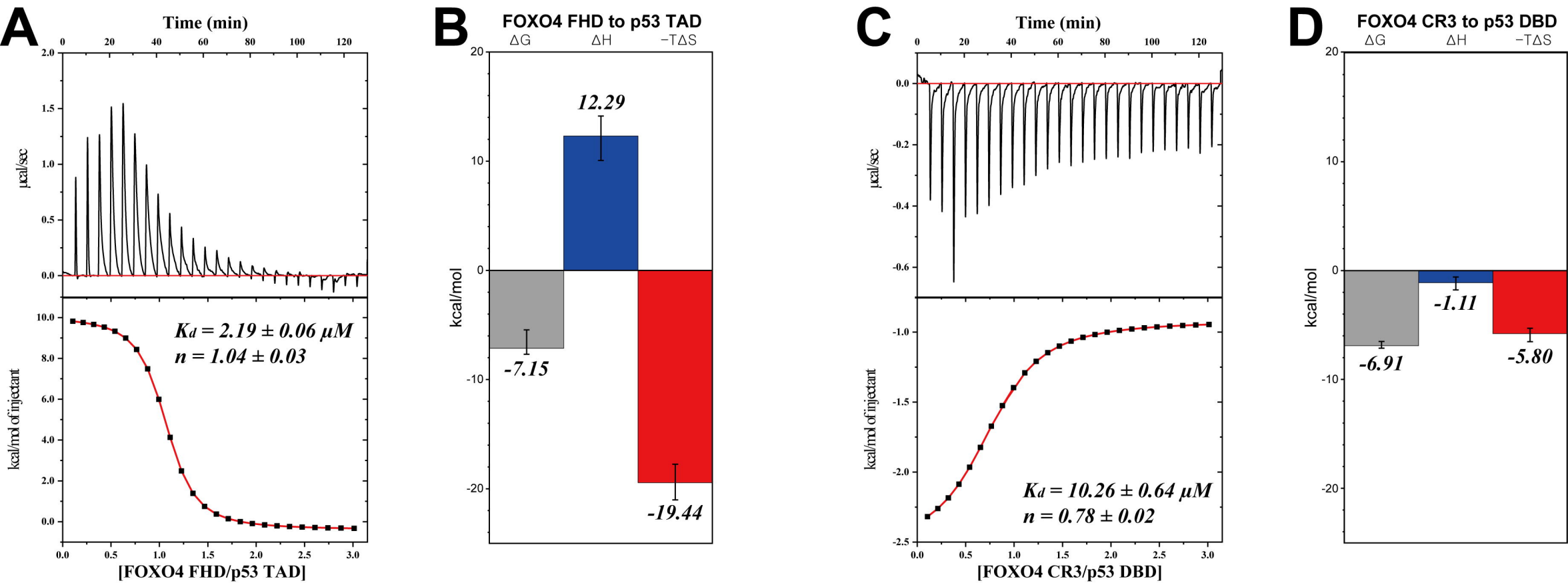
A
Time (min)
µcal/sec
kcal/mol of injectant
Kd = 2.19 ± 0.06 µM
n = 1.04 ± 0.03
[FOXO4 FHD/p53 TAD]
B
FOXO4 FHD to p53 TAD
ΔG
ΔH
−TΔS
kcal/mol
12.29
-7.15
-19.44
C
Time (min)
µcal/sec
kcal/mol of injectant
Kd = 10.26 ± 0.64 µM
n = 0.78 ± 0.02
[FOXO4 CR3/p53 DBD]
D
FOXO4 CR3 to p53 DBD
ΔG
ΔH
−TΔS
kcal/mol
-6.91
-1.11
-5.80

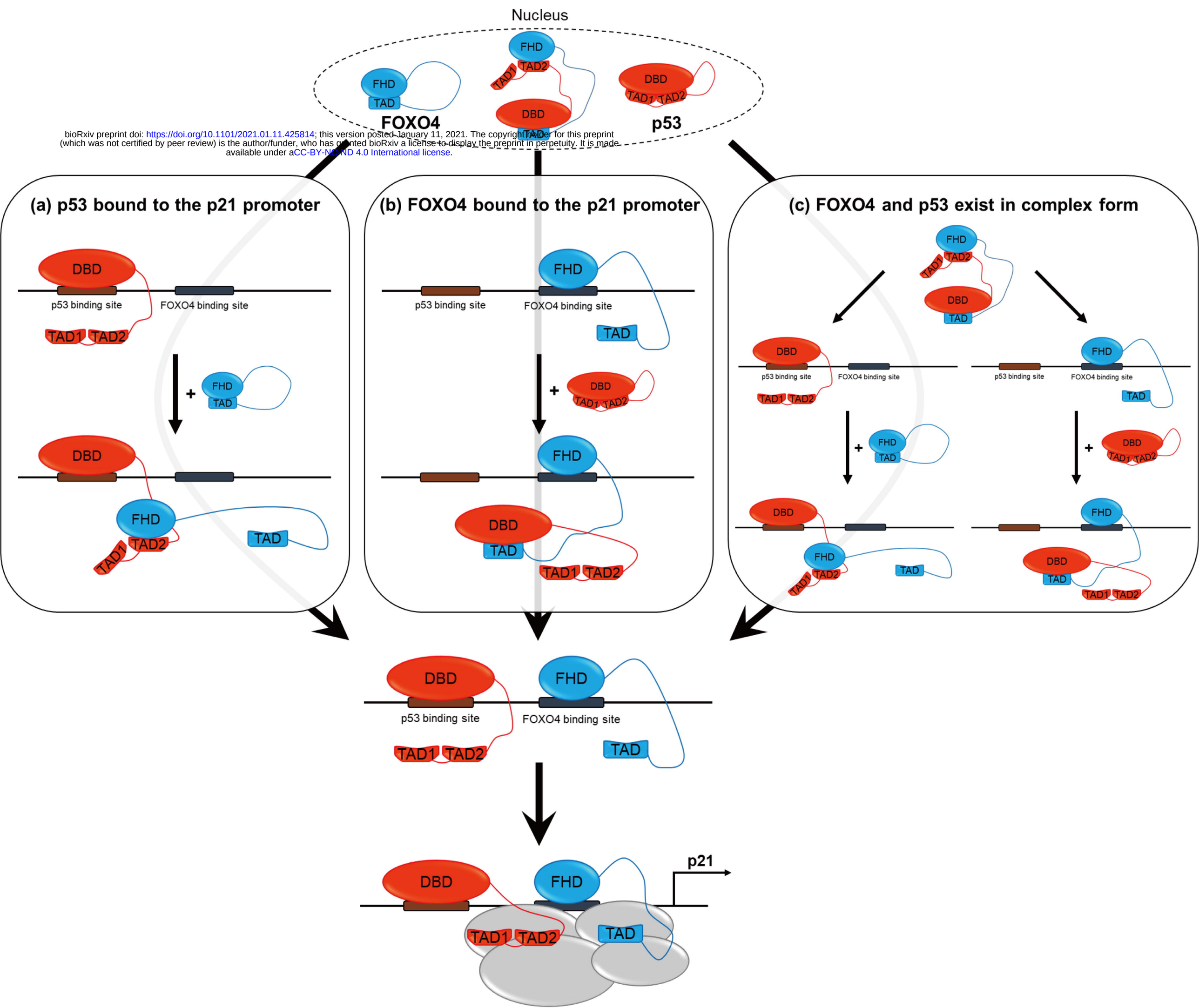

bioRxiv preprint doi: https://doi.org/10.1101/2021.01.11.425814; this version posted January 11, 2021. The copyright holder for this preprint (which was not certified by peer review) is the author/funder, who has granted bioRxiv a license to display the preprint in perpetuity. It is made available under aCC-BY-NC-ND 4.0 International license.